Advancements in branched bottlebrush polymers for responsive, targeted imaging

by

Molly A. Sowers

B.A., Cornell College (2012)

Submitted to the Department of Chemistry in Partial Fulfillment of the Requirements for the Degree of

Master of Science in Chemistry

at the

MASSACHUSETTS INSTITUTE OF TECHNOLOGY

February 2015

Signature of Author..... Signature redacted .....
Department of Chemistry
October 6, 2014

Certified by..... Signature redacted .....
Jeremiah A. Johnson
Assistant Professor of Chemistry
Thesis Supervisor

Accepted by..... Signature redacted .....
Robert Warren Field
Robert T. Haslam and Bradley Dewey Professor of Chemistry
Director of Graduate Studies

Advancements in branched bottlebrush polymers for responsive, targeted imaging

By

Molly A. Sowers

Submitted to the Department of Chemistry
On October 6, 2014 in Partial Fulfillment of the
Requirement for the Degree of
Master of Science in Chemistry

ABSTRACT

Multi-modality and stimuli responsive nanoparticles are promising platform materials for medical imaging and diagnostics. Specifically magnetic resonance imaging (MRI) and near-infrared (NIR) fluorescent probes can be used in combination to visualize biodistribution and *in vivo* clearance rates. We reasoned that through the use of a nitroxide radical MRI contrast agent along with a NIR fluorophore it would be possible to study these phenomena along with nitroxide reduction *in vivo*. Thus, we have developed branched bottlebrush copolymers that display compensatory fluorescence response to nitroxide reduction that enables correlation of MRI contrast, fluorescence intensity, and spin concentration in tissues. These polymers were synthesized by ring-opening metathesis copolymerization of two new branched macromonomers: one carries a bis-spirocyclohexyl nitroxide and the other the NIR dye Cy5.5. Promising preliminary results with the resulting polymers in solution MRI and NIR imaging studies as well as *in vitro* toxicity led us to explore the potential of these materials for *in vivo* applications.

Though nitroxide agents are promising organic agents for MRI applications, clinically, gadolinium-based MRI contrast agents are most common due to their high relaxivity and relatively low toxicity when bound to chelating ligands. We have also explored the idea of incorporation of gadolinium agents into our branched bottlebrush copolymer platform through the design of Gd-based branched macromonomers. While the fluorescence redox effects described in the nitroxide system above would not be applicable, chelated Gd could be used in much smaller concentration to provide similar MRI contrast. In this way, a small percentage of Gd could be added as an MRI tag to any polymer synthesized by ROMP.

A natural extension of the work described above is the incorporation of cellular targeting moieties for tissue-selective imaging. Toward this end, we propose the incorporation of known cellular targeting ligands onto the surface of branched bottlebrush polymers through the synthesis of end-functionalized branched macromonomers. The synthesis of several targeting ligands is described, alongside synthesis and characterization of positively charged nanoparticles for improved cellular uptake and ionic coordination of hyaluronic acid or other negatively charged polymers.

Thesis supervisor: Jeremiah A. Johnson
Title: Assistant Professor of Chemistry

TABLE OF CONTENTS

Chapter I. ORCAFluors: Responsive dual-modal MRI and near-IR imaging polymers

Introduction. Nanoparticle (NP)-based imaging agents have recently become pervasive in medical diagnostics research.[1-3] Of the common modalities, magnetic resonance imaging (MRI) and optical imaging are particularly common in clinical and research laboratories: MRI is used to image millions of patients per year,[4] while near-infrared (NIR) optical imaging is emerging as a powerful tool for image-guided surgery,[5] and is used routinely to monitor disease progression and nanoparticle biodistribution in animal models.[6,7]

Several examples of nanoparticle[8-13] and small molecule[14-17] MRI/NIR imaging systems have been previously reported. In some cases, stimuli-responsive constructs are reported to provide enhanced contrast or emission when exposed to specific cellular signals.[3,18,19] While these systems are often highly effective *in vitro* and *ex vivo*, short wavelength emitting fluorophores limit *in vivo* practicality.[20] Furthermore, these systems invariably rely on heavy metals to provide MRI contrast. While gadolinium-based agents are common in the clinic, they still face safety issues for certain patient populations.[21-23] In an effort to address the toxicity of Gd agents, we investigated organic radical contrast agents, specifically nitroxide radicals. Nitroxides have generally been considered too low contrast or too reactive *in vivo* for use in a clinical setting.[24,25] Conjugation of multiple nitroxides to a nanoscopic scaffold is a common strategy to address the former limitation;[26] increasing the

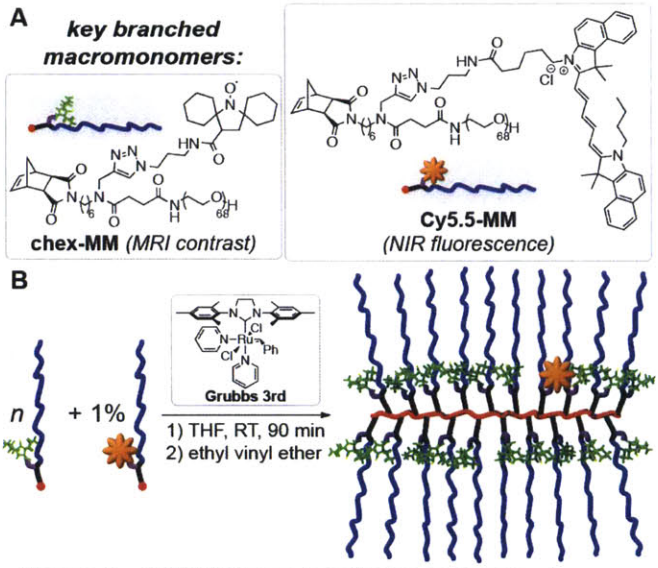

Figure 1. ORCAFluor synthetic scheme. A. Structures of branched MMs B. General procedure for ROMP synthesis of brush polymers

number of nitroxides per molecule increases the inherent molecular relaxivity of the probe. The latter issue can be addressed through the design of novel sterically shielded nitroxides. In 2013, the Rajca group reported an important advance by combining these concepts: they attached sterically shielded spirocyclohexyl nitroxides (**chex**) to nanoscale dendrimers.[27,28] These materials displayed MRI contrast *in vivo* up to 1 h after injection. Though this technique was effective, the dendrimer architecture limits the number of chemically addressable groups, which must be divided between solubilizing polyethylene glycol (PEG) chains and MRI active **chex**.

Previous work in the Johnson group has shown that ring opening metathesis polymerization (ROMP) of branched, nitroxide-conjugated macromonomers is an effective route to PEG-based branched bottlebrush polymers with a dense, sterically-shielded nitroxide core.[29] Along with functional group compatibility, ROMP provides excellent control over the average degree of polymerization (size), and often provides high conversion with low molar mass dispersity.[30-32] Using the branched macromonomer motif previously studied by the Johnson group also allows for one-to-one PEG to nitroxide loading, which ensures high solubility and shielding without sacrificing nitroxide density. Thus, we set out to create a PEG-based **chex** macromonomer (**chex-MM**, Figure 1) and a set of corresponding brush polymers for evaluation as organic MRI contrast agents.

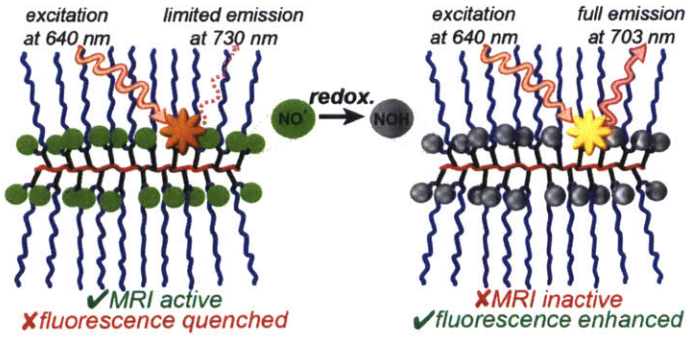

Figure 2. Redox response. Upon exposure to ascorbic acid, nitroxide radicals will be reduced. This renders the polymer MRI inactive, while enhancing fluorescent emission.

To further demonstrate the advantages of our approach, we sought to incorporate a second imaging handle into these systems through simple copolymerization. We chose to use a near-IR fluorophore that would provide *in vivo* fluorescence-based tracking of the polymer after nitroxide reduction (i.e., once the polymer is no longer MRI active). As displayed in Figure 2, the interaction between fluorophores and nitroxide radicals can be used as a type of redox activated on-off switch. There is extensive precedent for TEMPO quenching the fluorescence of excited singlet states *via* catalysis of intersystem crossing.[33-37] We attempted to utilize this quenching behavior by developing a polymer that would be MRI active in the radical form and fluorescent upon polymer reduction. Emission quenching is possible for a wide range of fluorophores, so we opted to use commercially available Cy5.5 (Figure 1), which has a maximum excitation at 675 nm and a maximum emission at 700 nm. Tissue absorption and background fluorescence is very low in this range,[38] which leads to a high signal-to-noise ratio.

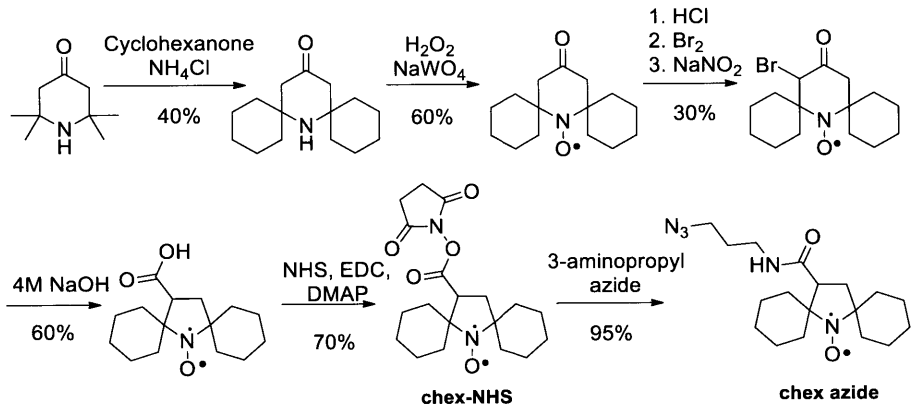

Scheme 1. Chex synthesis. Chex-NHS was synthesized according to literature procedures, then converted to an azide to perform "click" reactions.

Results and Discussion. In order to incorporate **chex** into our branched bottlebrush platform, we targeted the **chex-azide** shown in Scheme 1. **Chex-azide** can be synthesized via coupling of 3-aminopropyl azide and **chex-NHS**. The Rajca lab generously supplied **chex-NHS**

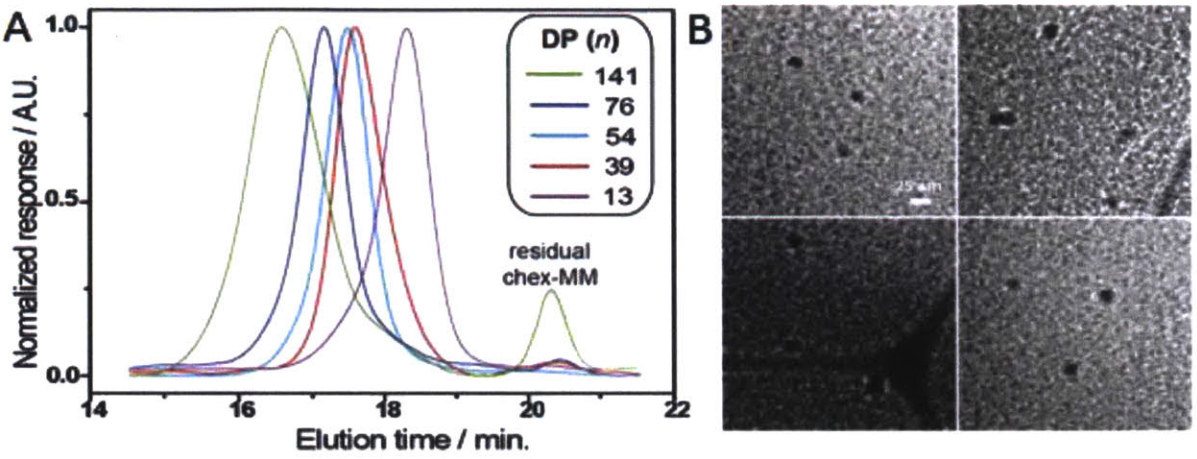

Figure 3. Polymer size characterization. A. GPC traces of several bottlebrush polymers derived from **chex-MM** with degree of polymerization *n*. B. Cryogenic transmission electron microscopy (Cryo-TEM) image of 55 unit bottlebrush polymer. Scale bar represents 25 nm.

for most of the following studies, though we have also conducted Rajca's original synthesis shown in Scheme 1. The *N*-hydroxy succinimidal ester was then easily displaced using 3-aminopropyl azide.[39] Copper(I)-catalyzed azide-alkyne cycloaddition (CuAAC) "click" chemistry was employed to couple **chex-azide** to **chex-MM** in near quantitative yield using CuOAc in DCM solvent,[30,40] with some product loss due from HPLC purification. Grubbs' 3rd generation bis(pyridyl) catalyst was used to perform ring opening metathesis polymerization (ROMP) of **chex-MM** to generate branched bottlebrush polymers with average degrees of polymerization ranging from 13-141. GPC traces of this series can be found in Figure 3A; cryogenic transmission electron miscroscopy (cryo-TEM, Figure 3B) and dynamic light scattering (DLS, Table 1) were performed to further characterize the 55 unit bottlebrush **P1** (Figure 3B).

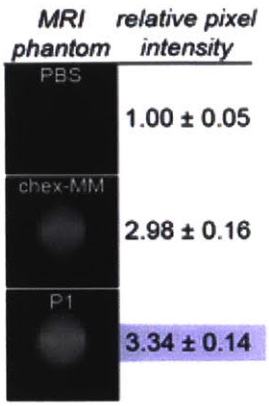

Figure 4. MRI phantoms. T1 weighted MRI of PBS, **chex-MM**, and **P1** polymers.

A T_1-weighted MRI phantom for **P1** (10 mM nitroxide in PBS) shows a 3.34 ± 0.14 fold enhancement compared to PBS alone (Figure 4). Longitudinal (r_1) and transverse (r_2) relaxivities for **chex-MM** and this series of polymers were measured using a Bruker 7 T MRI instrument (Table 1). The r_1 and r_2 values for **chex-MM** were 0.21 $mM^{-1}s^{-1}$ and 0.30 $mM^{-1}s^{-1}$, respectively. As expected for slowly diffusing NPs,[4,20] the polymers displayed increased relaxivity values. For example, the values for **P1** were r_1 = 0.32 $mM^{-1}s^{-1}$ and r_2 = 0.82 $mM^{-1}s^{-1}$, which correspond to 52% and 173% increases, respectively. The molecular relaxivities of **P1** can be obtained by multiplying the per nitroxide values by the average number of nitroxides per particle: r_{1mol} = 15.7 and r_{2mol} = 40.3 for **P1**. These values are comparable to clinically used metal-based contrast agents[19], likely enough to provide sufficient contrast for *in vivo* imaging applications. The degree of polymerization n = 55 sample was chosen for all subsequent polymer studies.

n	*Đ*	D_H *(nm)*	*r1* ($mM^{-1}s^{-1}$)	*r2* ($mM^{-1}s^{-1}$)
n.a. (chex-MM)	1.02	-	0.21	0.30
13	1.03	11.8	0.31	0.55
39	1.02	14.6	0.32	0.70
54 (**P1**)	1.05	16.8	0.32	0.82
76	1.08	18.0	0.36	0.84
141	1.30	21.0	0.31	0.51
proxyl	1.00	-	0.15	0.17
dendrimer	1.00	-	0.44	0.86
15XL star	1.28	19.2	0.45	3.07
20XL star	1.27	24.3	0.36	5.77

Table 1. Bottlebrush polymer characterization. Dispersity (GPC), hydrodynamic radius (DLS), and r_1 and r_2 relaxation parameters for brushes with varying degrees of polymerization (n). Proxyl refers to 3-carboxy-proxyl, and "dendrimer" refers to Rajca's previously studied polypropylenimine (PPI) nitroxide-conjugated fourth generation dendrimer.

With positive MRI contrast results, we turned toward the synthesis of a fluorescent Cy5.5-MM. It was unknown whether the poly-ene functionality of Cy5.5 would be compatible with ROMP. Furthermore, there were no previous reports of Cy5.5 fluorescence quenching by TEMPO. Starting with the Cy5.5 NHS ester, **Cy5.5-MM** (Figure 1) was synthesized analogously to **chex-MM**. Polymerization was then tested by adding 5% **Cy5.5-MM** with 95% nonfunctional **PEG-MM**. Overlapping refractive index and UV (675 nm) traces of the resulting polymer indicated complete incorporation of **Cy5.5-MM**. To examine the fluorescent properties of a dual-modal nitroxide/fluorophore, polymer **OF1** was polymerized via ROMP of 1% **Cy5.5-MM** and 99% **chex-MM** with a target degree of polymerization n = 55. This polymerization was performed on scales up to 250 mg in near-quantitative yield.

It has been shown that TEMPO can quench up to 64% of fluorescent emission of Cy5,[41] a similar cyanine dye to Cy5.5, when the two are covalently bound directly to each other; within our polymer construct, increased nitroxide-fluorophore distance led us to expect weaker interactions, though the increased number of nitroxides could be beneficial. Additionally, it was unclear to what extent the steric shielding of **chex** would affect emission quenching. To test these properties, a sample of **OF1**was added to pH 7.4 PBS buffer and excited at 640 nm. The emission at 703 nm (peak emission) was recorded and averaged over three samples. Sixty equivalents of sodium ascorbate, a major source of *in vivo* nitroxide reduction,[42,43] were added to the solution and the maximum emission was recorded, providing a 116% increase in fluorescence (Figure 5). In the presence of 10mM glutathione (GSH), addition of ascorbate affected fluorescence more drastically, up to a 248% increase (figure 5C). This behavior of co-reductants is not unexpected; while addition of GSH alone does not readily affect fluorescence, GSH reduces ascorbate radicals that could otherwise re-oxidize hydroxylamines and thereby turn

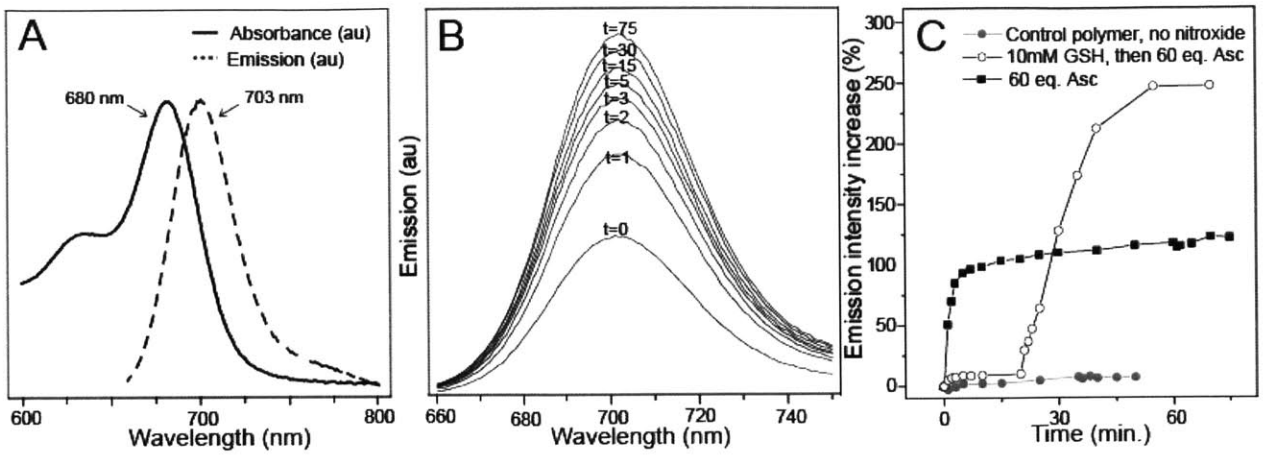

Figure 5. Fluorescent behavior of OF1. A. Absorbance and emission spectra of **OF1**. B. Emission change 0-75 minutes after addition of 60 eq. sodium ascorbate. C. Fluorescence increase after addition of sodium ascorbate or ascorbate with GSH. Control polymer with no nitroxides was also exposed to ascorbate reduction conditions, with negligible change in emission.

fluorescence off.[43] While the increase in fluorescence demonstrated by **OF1** is less than seen in many small molecule sensors, we reasoned that it would be suitable for initial *in vivo* study.

Prior to the proposed imaging studies, the toxicity of **OF1**was examined *in vitro* and *in vivo*. An MTT cell viability assay of **OF1** showed no toxicity to HeLa cells in concentrations up to 3 mg/mL, and *in vivo* tolerance was established in healthy BALB/c mice for doses up to 2000 $mg \cdot kg^{-1}$.[44] NIR images were obtained using IVIS (*In Vivo* Imaging System) of the live animals to demonstrate our ability to track biodistribution, and blood draws were performed to obtain pharmacokinetic information. The fluorescent load of **OF1** was enough to obtain quantitative clearance information, and prolonged blood circulation typical of this size nanoparticle was observed in a typical two-compartment fashion: an initial rapid 60% decrease in fluorescence was observed, followed by slow decay to 20% remaining fluorescence over 3 days.

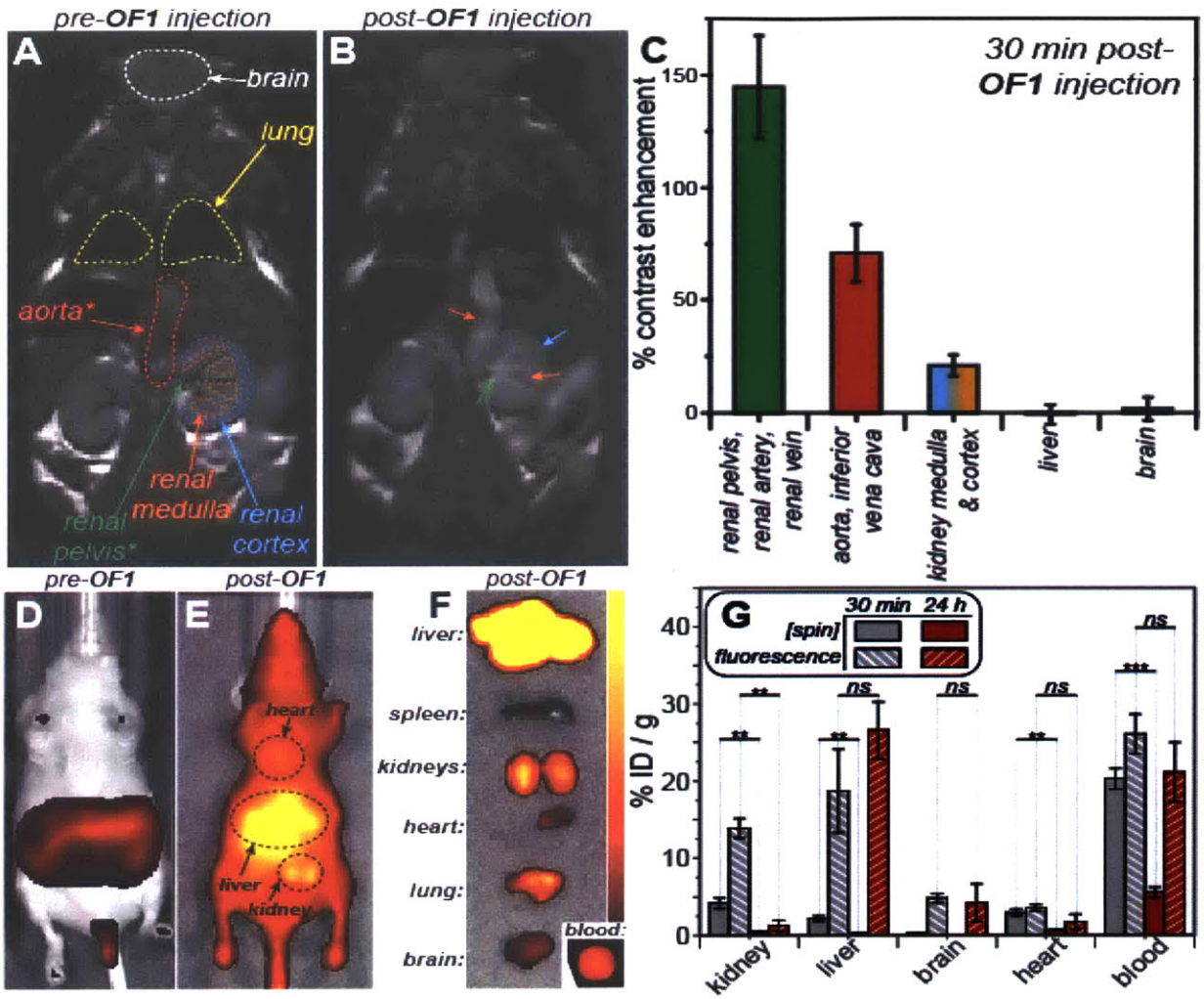

Figure 6. *In vivo* MR and IVIS images and quantification. A,B. Pre- and 30 min post-injection MR images. Noticeable contrast can be seen in the renal pelvis and aorta. C. MR contrast per organ. D,E. Whole animal IVIS pre- and post-injection. F. IVIS of organs 30 minutes post-injection. G. Fluorescence and EPR intensity of blood and homogenized organs at 30 minutes and 24 hours.

Next, *in vivo* imaging experiments were performed to examine MRI and fluorescence differences between pre-injection, 30 minutes, and 24 hours after dosing with **OF1**. By quantifying changes to the MRI contrast, spin concentration (as measured by EPR), and fluorescence intensity of the organs at these time points, we were able to obtain kinetic information about the organ-by-organ signal changes caused by reduction and biodistribution/clearance of **OF1**.

Before administration of **OF1**, MRI parameters for T1 weighting were optimized using an FSEMS (fast spin-echo multi-slice) pulse sequence, and animal autofluorescence was examined via IVIS. The fluorescent intensity of the **OF1** dose was measured to provide the total amount of injected fluorescence. All procedures involving animals were approved by the MIT Committee for Animal Care and monitored by Koch Institute Animal Imaging Core director Scott Malstrom. Four animals were used for each experiment.

Animals were anesthetized with 1-2% isoflurane, imaged *via* MRI and IVIS (Figure 6A, D) and administered (tail-vein injection) 30 mg **OF1** in 0.3 mL sterile PBS buffer. Animals were imaged again after 30 minutes (Figure 6B, E) or 24 hours and then sacrificed for organ collection. Fluorescence intensities were acquired for the heart, lung, liver, kidney, brain, spleen, muscle and blood (Figure 6F), and organs were frozen on dry ice and sent to our collaborators for spin concentration determination via EPR. As seen in Figure 6C, the highest MRI contrast at the 30 minute time point is found in the renal pelvis of the kidney, while the largest fluorescence signal was seen in the liver (Figure 6G). At 24 hours, the MRI contrast was drastically diminished, but fluorescence signals and significant spin concentrations were observed in certain tissues. PEG nanoparticles of this size are known to selectively accumulate in the liver.[45] These data suggest that appreciable concentrations of **OF1** can be found in the liver, but the EPR data suggest that the nitroxides are reduced in this organ, which is the location of ascorbate biosynthesis in mice. This hypothesis is supported by the comparatively low EPR signal in the liver, alongside previous work in nitroxide reduction kinetics.[46,47] Furthermore, the maximum MRI contrast and spin are observed in blood, which is expected given the extended blood circulation time of these PEG-based particles along with the very low concentration of ascorbate in blood.

The promising results displayed by **OF1** have led us to explore this nitroxide/Cy5.5 combination in other polymer architectures with the goals of increasing MRI contrast, the on/off signal-to-noise of the fluorescence probe, and introducing degradable groups into these architectures. Relaxivity is highly dependent on the hydrodynamic environment around the radical, as well as the tumbling rate of the particles as determined by the aspect ratio and size of a particle.[48] To alter these parameters, we have performed preliminary studies on two additional types of macromolecular architectures: random copolymer bottlebrush polymers and brush-arm star polymers (Figure 7). Copolymer bottlebrush polymers were created by synthesis of a small molecule analog of **chex-MM** labeled **Nb-chex**, and copolymerizing it with nonfunctional **PEG-MM** in varying ratios. Brush-arm star polymers (BASPs) were created from **chex-MM** and a bifuctional norbornene crosslinker synthesized by Jenny Liu.[31] By polymerizing short bottlebrush polymers and varying the number of added crosslinker (**XL**) equivalents, BASPs with a range of molecular weights were polymerized. GPC and DLS data were collected for each sample, and preliminary MRI studies were performed in the Jasanoff laboratory to measure r_1 and r_2 relaxivity (Table 1). While r_1 relaxivities were comparable to **OF1**, r_2 relaxivity for the star polymers saw a 7-fold increase over the highest previous measurement.

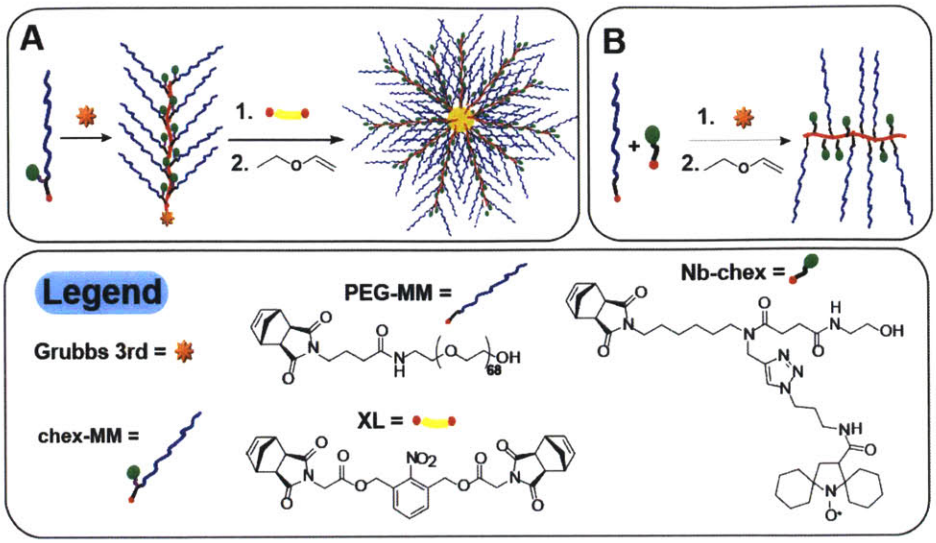

Figure 7. Structures and general procedures for polymer formation. A. **Chex-MM** to star and B. **Nb-chex** and **PEG-MM** to random copolymer brush.

Conclusions. A class of entirely organic, ascorbate-responsive, dual-modality molecular imaging agents was prepared using graft-through ROMP of novel spirocyclohexyl nitroxide and Cy5.5-conjugated MMs. Exposure of these materials to ascorbate leads to nitroxide reduction and enhanced fluorescence emission. *In vivo* studies confirmed significant MRI contrast enhancement (among the highest known for organic MRI contrast agents), as well as fluorescence emission that correlates with ascorbate concentration *in vitro* and *in vivo*. When viewed together, data from MRI, IVIS, and EPR suggest a correlation between ascorbate concentration and **OF1** fluorescence, confirming that **OF1** can be used to provide complementary information about *in vivo* redox processes. To our knowledge, this work represents the first example of an organic agent for dual ^{1}H MRI contrast enhancement and fluorescence imaging. The redox response and long circulation of these particles could make them applicable for tumor imaging studies; additionally, the modular synthesis is amenable to incorporation of targeting ligands or therapeutics.

Experimental Methods.

General Considerations. All reagents and solvents were purchased from Aldrich or VWR unless otherwise indicated. Bis-spirocyclohexylnitroxide-*N*-hydroxysucciniidyl (NHS) ester,[28] 3-aminopropyl azide[39], *exo*-norbornene alkyne-*branch*-NHS ester[30], and Grubbs 3rd generation bis(pyridyl) catalyst[49] were synthesized according to previously reported literature procedures. Anhydrous, deoxygenated dichloromethane (DCM) and tetrahydrofuran (THF) were used from solvent purification columns (JC Meyer).

Instrumentation information. ^{1}H and ^{13}C nuclear magnetic resonance (^{1}H NMR) spectra were obtained from Bruker AVANCE-400 NMR spectrometers at MIT. NMR spectra were analyzed using MestReNova NMR 8.0.1 software and referenced to the residual chloroform peak at 7.26 ppm.

Electron Paramagnetic Resonance (EPR) spectra were obtained at the University of Nebraska using a Bruker CW X-band spectrometer, equipped with a frequency counter. The spectra were obtained using a dual mode cavity; all spectra were recorded using an oscillating magnetic field perpendicular (TE_{102}) to the swept magnetic field. 2,2-diphenyl-1-picrylhydrazyl (DPPH) powder ($g = 2.0037$) was used as a g-value reference.

Gel permeation chromatography (GPC) analysis was performed on an Agilent 1260 LC system equipped with an Agilent multi-wavelength UV/Vis detector, Wyatt T-rEX refractive index detector, Wyatt DAWN EOS 18-angle light scattering detector, and two Shodex KD-806M GPC columns. The GPC system was equilibrated at 60 °C with a 1 mL/min flow rate of DMF with 0.025 M LiBr.

Dynamic light scattering (DLS) measurements were taken at room temperature using a Wyatt Technology DynaPro Titan DLS. Samples were dissolved in phosphate buffered saline solution, passed through a 0.4 μm nylon syringe filter into a 0.3 mm cuvette. Average hydrodynamic radii were obtained using Dynamics V6 software from DynaPro Wyatt Technologies. DLS correlation curves were fit using the CONTIN algorithm.

Matrix-assisted laser desorption/ionization time-of-flight (MALDI-TOF) analyses were collected on a Bruker OmniFlex instrument with a 337 nm N_2 laser with a 0.1 nm spectral bandwidth.

Liquid chromatography-mass spectrometry (LC-MS) data were obtained on an Agilent 1260 LC system with an Agilent 6130 single quadrupole mass spectrometer with a HALO column using linear gradients of 0.1% acetic acid in nanopure water (v/v%) and acetonitrile.

Preparative high-performance liquid chromatography (prep-HPLC) purification was performed on a Beckman Coulter System Gold HPLC with a 127 solvent pump module and 166P detector set to detect at 210 nm. A linear gradient from 95:5 (v:v%) 0.1% AcOH in H_2O (v:v%): MeCN to 5:95 (v:v%) 0.1% AcOH in H_2O (v/v%): MeCN over 9-14 minutes was used for separation.

Absorbance measurements were collected on a Varian Cary 50 Scan UV/Vis spectrophotometer and analyzed using Cary WinUV software in nanopure water. Fluorescence data were taken on a Horiba Jobin Yvon Fluorolog-3 fluorometer using a 450 W Xe lamp and right-angle detection.

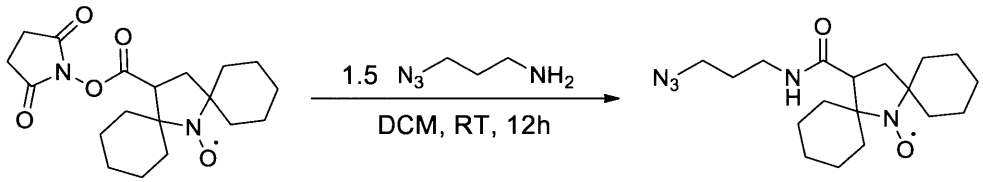

Bis-spirocyclohexylnitroxide-propyl-azide. Bis-spirocyclohexylnitroxide-*N*-hydroxysuccinimidyl (NHS) ester (60 mg, 0.17 mmol) was added to a vial containing 3-aminopropyl azide (80 µL of 3M solution in toluene, 0.24 mmol) in 1 mL dry DCM. The reaction was stirred for 1 hour, then transferred to a silica gel column and purified via flash chromatography with 5% methanol in DCM. Product containing fractions were determined by LC-MS, combined, dried over $MgSO_4$, and condensed on a rotary evaporator. The yellow

residue was dried under vacuum to give the desired product as a yellow oil in 95% yield. ^{1}H NMR is provided below in Figure S13. DART-HRMS calculated for $C_{18}H_{30}N_5O_2$ $[M+H]^+$ 349.247, observed 349.2467. ^{1}H NMR (400 MHz, CD3OD, r.t.): δ 1.36 (s, 2H), 1.62 (m, 5H), 2.24 (s, 2.2H), 2.77 (m, 3H), 3.40 - 4.15 (m, 12H), 4.66 (s, 1.5H), (6.39 (s, 0.1H).

Poly(ethylene glycol) monoamine (PEG-NH_2):

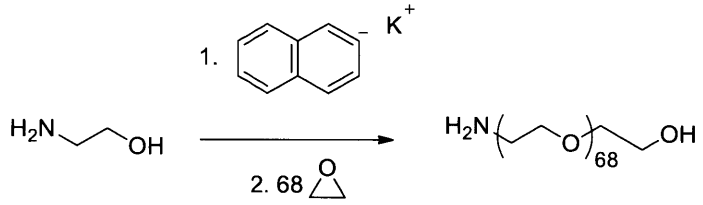

Reaction Setup: A lecture flask of ethylene oxide (EO) was connected in series to a graduated vessel (for EO drying, *vide infra*), and a reaction flask. Teflon tubing was used to connect the vessels, all stir bars were pyrex coated, and all joints were lubricated with fluorinated grease. All portions of the reaction setup were carefully kept under nitrogen at all times and isolated from one another until otherwise indicated. A blast shield was placed in front of any vessel containing EO.

Potassium naphthalenide initiator: An oven-dried 100 mL Shlenck flask equipped with a pyrex stirbar was evacuated and refilled with nitrogen three times. Potassium metal (0.92 g, 23.6 mmol) was cut under mineral oil and transferred with tweezers to a vial containing dry cyclohexane. Potassium was transferred to a second vial of clean cyclohexane to remove any residual mineral oil, and then added quickly to the Schlenk flask. Residual cyclohexane was removed by vacuum (30 min). Napthalene (3.30 g, 25.8 mmol, 1.1 eq) was then added to the

Schlenk flask, which was briefly evacuated and refilled with nitrogen. Dry THF (23.6 mL) was added; the solution immediately began to turn dark green as potassium dissolved. The flask was covered with aluminum foil and stirred at room temperature for 2 h. The initiator concentration was tested by titration against 0.10 mL (1.3 mmol) isopropanol in 10 mL THF. After adding 1.40 mL of initiator, the dark green initiator color remained for over ten seconds, indicating a concentration of 0.93 M. The initiator was stored in the aluminum covered Schlenk flask for up to three days before use.

Calcium hydride (1 g) was added to the drying vessel (labeled b in Supplementary Fig. 12). An ice bath was placed around the drying vessel, the EO tank was opened slowly and EO was allowed to condense in the drying vessel. Once 22 mL (440 mmol) of liquid EO had accumulated, the EO lecture flask was closed, isolated from the drying vessel, and removed from the hood. The ice bath was maintained around the drying flask as redistilled aminoethanol (0.40 mL, 6.6 mmol) and dry THF (45 mL) were added to the reaction flask through a rubber septum. Potassium naphthalenide solution (7.10 mL of 0.93 M, 6.6 mmol) was added, and the mixture became white and cloudy; the precipitated potassium aminoethanoxide was washed from the flask walls with 5 mL THF. The ice bath was then removed from the drying vessel and placed around the reaction flask. The drying vessel was opened to the reaction flask, and the EO was allowed to boil and slowly distill into the reaction flask. Once the drying flask was empty, the reaction vessel was sealed, the ice bath was removed, and the reaction was allowed to warm to room temperature. The polymerization was stirred at room temperature for 72 h. After this time, 6.6 mmol of hydrochloric acid (5.3 mL of 1.25M HCl in methanol) was added dropwise to the reaction. The flask was then opened to air and stirred for 1 h. The reaction mixture was then

poured directly into 700 mL of cold diethyl ether and stored at -20° C for 1 h. The white precipitate was vacuum filtered, redissolved in 70 mL of toluene, and precipitated in cold ether again. After a second filtration, the polymer was vacuum dried overnight to remove all residual solvent, providing a powdery white solid in 92% isolated yield. ^{1}H NMR spectrum is shown below.

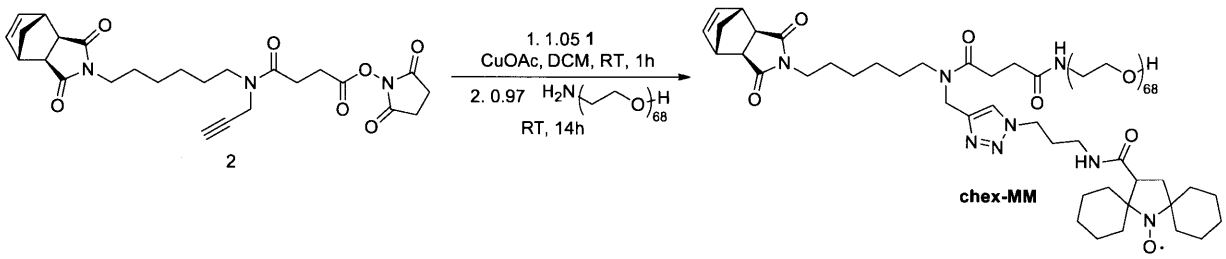

Chex-MM. Compound **2** (37.4 mg, 75 mmol) was added to a vial with azide **1** (27.6 mg, 79 mmol) and 3 mL dry DCM under N_2. A spatula tip of CuOAc was added and the vial was flushed with N_2. After five minutes, LC/MS analysis of the reaction indicated nearly complete conversion of **2** to the intermediate triazole-*branch*-NHS compound. Solid PEG-NH_2 (220 mg, 73 mmol) was then added to the reaction and the mixture was stirred for 14 h. The entire reaction mixture was dried on a rotary evaporator, redissolved in MeOH (3 mL), passed through a 0.4 □m Nylon syringe filter, and subjected to prep-HPLC. The pure fractions containing **chex-MM** were condensed with a rotary evaporator. The resulting residue was dissolved in dichloromethane (DCM), dried over Na_2SO_4, condensed on a rotary evaporator, and dried overnight under vacuum to yield a light yellow solid in 65% yield. MALDI spectrum is shown in Supplementary Fig. 1, and ^{1}H NMR is provided in Supplementary Fig. 15. ^{1}H NMR (400 MHz, CD3OD, r.t.): δ 1.27 (m, 6H), 1.52 (m, 6H), 2.14 (s, 10H), 2.55 (s, 2H), 2.69 (m, 3H), 3.28 (s, 2H), 3.48 (m, 6H), 3.66 (m, 220H), 3.85 (t, 2H), 6.30 (s, 2H), 6.51 (s, 1H).

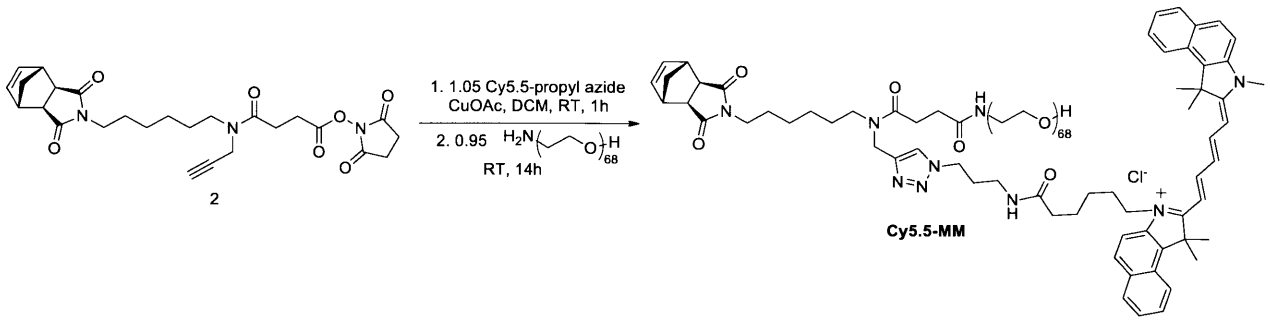

Cy5.5-MM. Compound **2** (1.3 mg, 2.6 mmol) was added to a vial with Cy5.5-propyl azide (Kerafast, 2 mg, 2.8 mmol) and 1 mL dry DCM under N_2. A spatula tip of CuOAc was added and the vial was flushed with N_2. After five minutes, LC/MS analysis of the reaction indicated nearly complete conversion of **2** to the intermediate Cy5.5-*branch*-NHS compound. Solid PEG-NH_2 (7.7 mg, 2.5 mmol) was then added to the reaction and the mixture was stirred for 14 h. The entire reaction mixture was dried on a rotary evaporator, redissolved in MeOH (0.7 mL), passed through a 0.4 □m Nylon syringe filter, and subjected to prep-HPLC. The pure fractions containing **Cy5.5-MM** were condensed with a rotary evaporator. The resulting blue residue was dissolved in dichloromethane (DCM), dried over Na_2SO_4, condensed on a rotary evaporator, and dried overnight under vacuum to yield a blue solid in 77% yield. The MALDI spectrum is shown in Supplementary Fig. 1, and the ^{1}H NMR is shown in Supplementary Fig. 16. ^{1}H NMR (400 MHz, CD3OD, r.t.): δ 1.15-1.29 (m, 7H), 1.42-1.58 (m, 8H), 1.76 (s, 2H), 2.20-2.55 (m, 18H), 2.64 (d, 4H), 3.24 (m, 6.5H), 3.39 (m, 6.5H), 3.63 (m, 305H), 4.18 (s, 2H), 4.40 (m, 2H), 4.54 (s, 2H), 6.25 (m, 3H), 6.37 (m, 1H), 6.72 (m, 1H), 7.39 (t, 2H), 7.48 (m, 2H), 7.61 (t, 2H), 7.93 (m, 6H), 8.07 (m, 2H).

Branched bottlebrush synthesis by ROMP: All polymerizations were performed in a glovebox under N_2 atmosphere. All reported brushes were made in the same manner; the method described below is specific to **OF1**, but can be generalized by varying monomer and catalyst equivalents.

Chex-MM (198 mg, 0.05 mmol) and **Cy5.5-MM** (2.0 mg in 20μL, 0.5 μmol) were combined in a 4 mL vial and dissolved in 0.795 mL THF. A solution of Grubbs 3rd generation bispyridine catalyst (0.278 mL of 4 mg / mL catalyst solution, 1 μmol) was added to the vial and stirred for 90 minutes. The reaction was quenched with a drop of ethyl vinyl ether; a small aliquot was taken for GPC characterization, and the rest was transferred to a 15 kDa molecular weight cutoff dialysis tubing (Spectrum Laboratories) with 5 mL of Millipore water. The polymer was dialyzed against 500 mL of Millipore water (3 rounds of fresh water were added with 2 h between each solvent exchange) with gentle stirring to remove any unreacted MM. The polymer solution was then lyophilized to dryness, and stored in the dark at 4 °C.

Fluorimetric analysis of nitroxide quenching: Analysis of Cy5.5 fluorescence quenching within spirocyclohexyl nitroxide-functionalized polymers was performed by monitoring excitation and emission at 640 nm and 703 nm, respectively. Slit widths of 5 nm for excitation and 7 nm for emission were used for all studies. Polymer samples (OF1 or control polymer with no nitroxide) were dissolved in 2 mL of pH 7.4 1X PBS buffer; UV/Vis and fluorescence spectra were collected. Aliquots of ascorbic acid were then added to the cuvette as outlined in Fig. 3B. Emission spectra were repeatedly obtained until no change was observed. A representative series of spectra are shown in Figure 5. Note: The pH was measured before and after ascorbic acid addition; the values were 7.0 and 6.31 respectively. The absorption/emission properties of Cy5.5 are not pH dependent.

Phantom relaxivities by MRI: Monomers and polymers were completely transferred as solids using dichloromethane to another set of accurately weighed clean vials, and then evacuated to a constant mass in Schlenk containers (1 mTorr-vacuum). For selected monomers and polymers, small samples (0.4 – 0.8 mg) were examined by ^{1}H NMR spectroscopy in chloroform-*d* (500 MHz, cryoprobe, 3-mm tubes); only monomer **MM1** had a very small residue of dichloromethane, and all other samples, examined by NMR spectroscopy, were solvent free.

To each vial containing the sample remaining after evacuation and NMR spectra, 0.5 mM PBS (0.800 mL, pH 7.2 checked with pH meter) was added, to provide homogenous-to-turbid stock solutions. Spin concentration of stock solutions was determined by EPR spectroscopy. Serial dilution (100 – 10% in 10% increments) of each stock solution provided an array of ten 0.1 mL-samples in PCR tubes; for each T_1 and T_2 measurement of ^{1}H in water, the array of ten 0.1-mL samples and 0.1-mL sample of buffer (11 PCR tubes) were used.

T_1 and T_2 measured at the University of Nebraska Medical Center were obtained using coronal T_1 and T_2 map imaging protocols. T_1 mapping was done using a progressive saturation RARE T_1 mapping measurement with RARE factor = 4, First TE and spacing of 6.4 ms, TR= 10000, 5000, 3000, 1500, 1200, 800, 500, 450, 400, 350, and 300 ms, 60 mm field of view (FOV), 1 mm slice thickness, one slice for a total acquisition time of 10 min. T_2 mapping was done using CPMG phase cycled multiecho imaging of all sample concentrations including buffer in a single image. Acquisition parameters were: 10 echo, TE=10 ms, one 1mm thick slice, 256 x 128 matrix, 1 average, 3000 ms repetition time, 60 mm FOV, for a total acquisition time of 10 min. T_1 and T_2 values were extracted from each sample in the image using regions of interest in the image sequence analysis tool in Paravision 5.1. T_2 values were determined by using the even

numbered echoes, fitting the noise floor using the highest free radical concentration, and fixing the value for the remaining samples in each image.

Signal Intensity as a function of relaxivity: During MRI acquisition time, T_1 weighting is accomplished by use of a short repetition time (TR) relative to the T_1 of the imaged sample or tissue. After several pulses (dummy pulses) a steady state magnetization is established which has an intensity (M_{ss}) relative to the maximum signal intensity (M_0) of: $\frac{M_{ss}}{M_0} = \frac{(1-e^{-TR/T_1})sin\alpha}{(1-e^{-TR/T_1}cos\alpha)}$, where α = excitation flip angle. The images acquired for Figure 4 were obtained using a fast spin echo sequence (α=90°) with a TR of 500 ms. T_1 of the PBS was measured as 2,770 ms. The molar T_1 relaxivity (r_1) of **chex-MM** was found to be 0.208 $mM^{-1}s^{-1}$ and the molar relaxivity of **P1** was found to be 0.318 $mM^{-1}s^{-1}$. Thus for the three samples in Figure 4, PBS, 10 mM **chex-MM** in PBS, and 10 mM **P1** in PBS, the T_1's of the samples were: $1/T_1 = 1/T_{1PBS} + r_1*(10\ mM)$ which comes to 2770 ms (PBS), 410 ms (**chex-MM**), and 282 ms (**P1**). This results in M_{ss}/M_0 values for the three samples of 0.165 (PBS), 0.704 (**chex-MM**), and 0.830 (**P1**). Normalizing the intensity of PBS to 1, this gives relative signal intensities of 4.26 (**chex-MM**) and 5.03 (**P1**). However, this relative signal intensity does not include decay due to T_2. The RARE (fast spin echo) sequence used a four-echo train with the central k-space echo at an echo time (TE) of 8.9 ms. Signal intensity loss due to T_2 loss is given my $M_{T2}/M_{ss} = e^{-TE/T2}$. The T_2 of PBS is 325 ms. Molar T_2 relaxivity (r_2) of chex-MM was found to be 0.300 $mM^{-1}s^{-1}$ and the molar relaxivity of P1 was found to be 0.821 $mM^{-1}s^{-1}$. Thus for the three samples in Figure 4, PBS, 10 mM **chex-MM** in PBS and 10 mm **P1** in PBS, the T_2's of the samples were: $1/T_2 = 1/T_{2PBS} + r_2*(10\ mM)$ which comes to 325 ms (PBS), 165 ms (**chex-MM**), and 89 ms (**P1**). Thus T2 signal loss for this sequence in each sample resulted in M_{T2}/M_{ss} = 0.97 (PBS), 0.95 (chex-MM), and 0.90 (P1).

Normalizing PBS to 1 and taking into account the steady state magnetization, this results in final signal intensities of 4.17 (**chex-MM**) and 4.67 (**P1**), a bit higher than the measured values, but consistent with a 12% contrast enhancement seen with **P1** over **chex-MM**. Note that the T_2 decay calculation does not take into account the multiple echo train, but only includes the first echo, which should dominate the signal intensity in the center of k-space.

Cell culture and in vitro toxicity: HeLa cells (ATCC) were maintained in MEM Media supplemented with 1% penicillin/streptomycin and 29% fetal bovine serum in 5% CO2 humidified atmosphere (37° C). Cells were plated in 96-well plates at 10,000 cells per well and grown for 24 h before treating with varied concentrations of polymer. Each polymer concentration was represented by four replicate wells. After 48 h, the cells were incubated for 4 h with thiazolyl blue tetrazolium bromide (MTT). Reduced thiazoyl tetrazolium formazan was then solubilized with dimethyl sulfoxide (DMSO), and cell viability was calculated based on absorbance at 550 nm.

Animal usage: All procedures involving animals were reviewed and approved by the MIT Committee for Animal Care. Toxicity and pharmacokinetics studies were performed on healthy female BALB/c mice, aged 12-16 weeks. MRI studies were performed on healthy female NCR nude mice receiving and alfalfa free diet to minimize autofluorescence. All studies involving animals were performed on groups of n=4 or n=5 to provide statistical significance. Exclusion criteria included human error in NP administration.

***In vivo* toxicity and pharmacokinetics:** Eight polymer solutions ranging from 0.1 – 40 mg of **OF1** in sterile pH 7.4 PBS buffer were prepared. To find a rough toxicity threshold, solutions were first administered to one mouse per particle solution. NP solutions were passed through a 0.2 micron filter before being injected slowly via catheter into the tail vein. Upon seeing that the polymer was well tolerated by all animals, two groups of 5 animals were dosed with 30 or 40 mg of **OF1**. Animals receiving 40 mg of **OF1** demonstrated higher weight loss and some initial lethargy, while animals receiving 30 mg displayed no adverse physical effects; this dosage was used for all subsequent imaging studies.

***In vivo* MRI and IVIS:** Live animal MRI experiments were conducted at the Koch Institute for Integrative Cancer Research at MIT in a Varian 7T/310/ASR-whole mouse MRI system. T1 weighted MR images were collected using the fast spin echo multiple slices (FSEMS) pulse sequence with minimum repetition time (TR) = 739 ms, ESP = 9.52 ms, ETL = 4, a 256x256 matrix, and 4 averages over 18 slices at 1 mm thickness. Scans were collected with respiratory gating (PC-SAM version 6.26 by SA Instruments Inc.) to avoid confounding noise due to chest movement. Respiratory rate and animal temperature were closely monitored during image collection.

In vivo fluorescence images were obtained on an IVIS Spectrum bioluminescent and fluorescent imaging system from Xenogen. Excitation and emission values (640 nm, 700 nm respectively) were kept constant, and exposure times from 2-10 seconds were used to obtain clear images. Epi-fluorescence is reported in radiant efficiency and used only as comparison between pre- and post-injection values.

MRI and IVIS images were obtained for each animal (n=4) before administration of **OF1**. Mice were fit with tail vein catheters and slowly injected with **OF1** solution. Thirty minutes or 24 hours after injection was complete, mice were reimaged with both IVIS and MRI, then immediately sacrificed in a CO2 chamber for tissue collection and fluorescence imaging. Organs were briefly washed with saline to remove any exogenous blood from the dissection process.

***In vivo* MRI and IVIS data analysis:** A region of interest (ROI) around each organ was manually selected for a given image slice. The average intensity and are of the ROI were measured. This procedure was repeated for each image slice where the organ/tissue was visible. Using Excel (Microsoft), the average intensity of each ROI was multiplied by its area. These values were then summed together for all image slices of a given organ. This sum was divided by the sum of the ROI areas for the same organ to provide the volume-average intensity. The same procedure was repeated for images of 4 mice collected before and 30 min after injection of **OF1** (8 images total). Volume averaged intensity increases (shown in Figure 4C) were obtained by subtracting from the following equation: ((contrast 30 min after injection) – (contrast before injection)) / (contrast before injection) * 100%. The values for % contrast enhancement were normalized by the muscle, which was assumed to be zero. Note that this normalization changed the final values by less than 10%.

***Ex vivo* fluorescence methods:** After collecting *in vivo* MRI and fluorescence data (*vide supra*), mice were sacrificed in a CO_2 chamber and immediately dissected to remove kidneys, liver, spleen, heart, lungs, brain, and a section of flank muscle tissue. Organs were quickly washed with PBS buffer to remove excess blood from the necropsy process.

Extracted organs were placed on a black, non-emitting background for fluorescence analysis. IVIS parameters were maintained from *in vivo* measurements. Excitation and emission values (640 nm, 700 nm respectively) were kept constant, and exposure times from 2-10 seconds were used to obtain clear images, and scaled to photons per second for all comparisons.

***Ex vivo* EPR spectroscopy:** Throughout the *ex vivo* EPR spectroscopy section, labels "YW1133r3-6" and alike correspond to sample or experiment codes directly traceable to the laboratory notebooks or raw data.

The animal tissues were shipped in dry ice from MIT to Nebraska in centrifuge tubes; upon receiving, the tubes were stored in liquid nitrogen. For preparation of EPR samples, the tissues samples were temporarily moved from the liquid nitrogen storage to dry ice. Each tissue sample, one at a time, was rapidly thawed, and then transferred to a weighed vial. Then, 0 – 500 μL of PBS buffer (0.5 mM, pH = 7.2) was added. The sample with PBS was then put into an ice-water bath and homogenized with rotor stator homogenizer, and then pipetted to a 4-mm O.D. EPR sample tube. The samples were degassed by sonication, as needed (e.g., when gas bubbles were visible). The EPR tube was capped, sealed with parafilm, and then stored briefly in acetone-dry ice bath prior to the measurement of spin concentration.

The spin concentrations of nitroxide radicals in tissues (μmol/g, μmol of $S = ½$ nitroxide radical per gram of tissue) were measured at –30 °C (243.2 K), to increase signal-to-noise for the aqueous samples. Measurements of the tissue samples were alternated with the measurements of the references for spin concentration (see: next paragraph) and *g*-value (DPPH powder as a *g*-value reference). For tissue samples with low signal-to-noise, the cavity background was recorded with identical parameters as for the tissue sample (including identical number of scans

and identical receiver gain). Typical parameters were as follows: microwave attenuation (20 dB), modulation amplitude (5 Gauss), spectral width (300 Gauss), resolution (512 points), conversion (40.96), time constant (10.24), and sweep time (20.97 sec.); these parameters were kept identical for the tissues, references, and cavity backgrounds. The number of scans (NS = 8 – 256) and receiver gain (RG) were adjusted as needed for each sample.

The reference for spin concentration was prepared from the same branched bottlebrush polymer as used for injection to mice. The polymer was dissolved in PBS (0.5 mM, pH 7.2) to provide 1.036 mM solution, for which concentration was calibrated with 3-carboxy-PROXYL in PBS buffer (0.5 mM, pH 7.2) at ambient temperature (295.0 K). Except when during the measurement, this reference was always stored in dry ice, and occasionally re-checked for spin concentration decay.

							Relaxivity			
Nitroxide	MM	Target DP	Mn from GPC	PDI	Actual DP	Rh / DLS	r1	R^2	r2	R^2
	alk-PEG3000	10	29760	1.086	8a					
	alk-PEG3000	25	79870	1.023	22a					
	alk-PEG3000	50	298500	1.04	81a					
	alk-PEG3000	100	789300	1.16	215a					
	alk-PEG1600	10	33060	1.04	15a					
	alk-PEG1600	25	70040	1.031	31a	150(11)				
TEMPO	alk-PEG1600	50	288700	1.083	127a					
	alk-PEG1600	100	606600	1.172	268					
	peg4-PEG3k	10	50900	1.087	13a	11(1)	0.277	0.9995	0.353	0.9921
	peg4-PEG3k	25	122200	1.096	32a	7(0.1)				
	peg4-PEG3k	50	314700	1.197	83a	5.1(0.1)				
	peg4-PEG3k	100	328600	1.69	87a	17(1)				
	peg4-PEG1.6k	10			0					
	peg4-PEG1.6k	25			0					
	peg4-PEG1.6k	50			0					
	peg4-PEG1.6k	100	312900	1.34	131a	153(7)				
	alk-PEG3000	10	47570	1.016	13b		0.321	0.9991	0.698	0.9963
	alk-PEG3000	25	145600	1.03	39b		0.314	0.9994	0.554	0.9982
	alk-PEG3000	50	284800	1.078	76b		0.359	0.9993	0.841	0.9982

	alk-PEG3000	100	526800	1.296	141b		0.305	0.9997	0.514	0.9835
	alk-PEG1600	10	82980	1.051	35b	5.2(0.3)	0.314	0.998	0.65	0.9982
	alk-PEG1600	25	273600	1.6	116b	15(1)				
CyHex	alk-PEG1600	50	322300	1.33	136b	16(1)	0.292	0.999	0.597	0.998
	alk-PEG1600	100			0					
	peg4-PEG3k	10	77750	1.03	20b	9(0.2)				
	peg4-PEG3k	25	158300	1.043	41b					
	peg4-PEG3k	50	267300	1.126	69b					
	peg4-PEG3k	100			0					
	peg4-PEG1.6k	10			0					
	peg4-PEG1.6k	25			0					
	peg4-PEG1.6k	50			0					
	peg4-PEG1.6k	100			0					
PPI	yw08-53-3	G4 PPI CyHx dend					0.438	0.9995	0.855	0.9963
dendr	yw04-27-3	G2 PPI CyHx dend					0.295	0.9985	0.498	0.9405
	yw04-25-3	G3 PPI CyHx dend					0.426	0.9989	0.673	0.9972
	PROXYL	reference					0.149	0.998	0.174	0.9933
PEG-4	yw08-89crp2	Me4 PEG4 acid					0.142	0.999	0.172	0.9941

Table 2. Extended Bottlebrush polymer characterization. A list of polymerized MRI active bottlebrush polymers, compared to several standards provided by the Rajca lab.

Spectral Data.

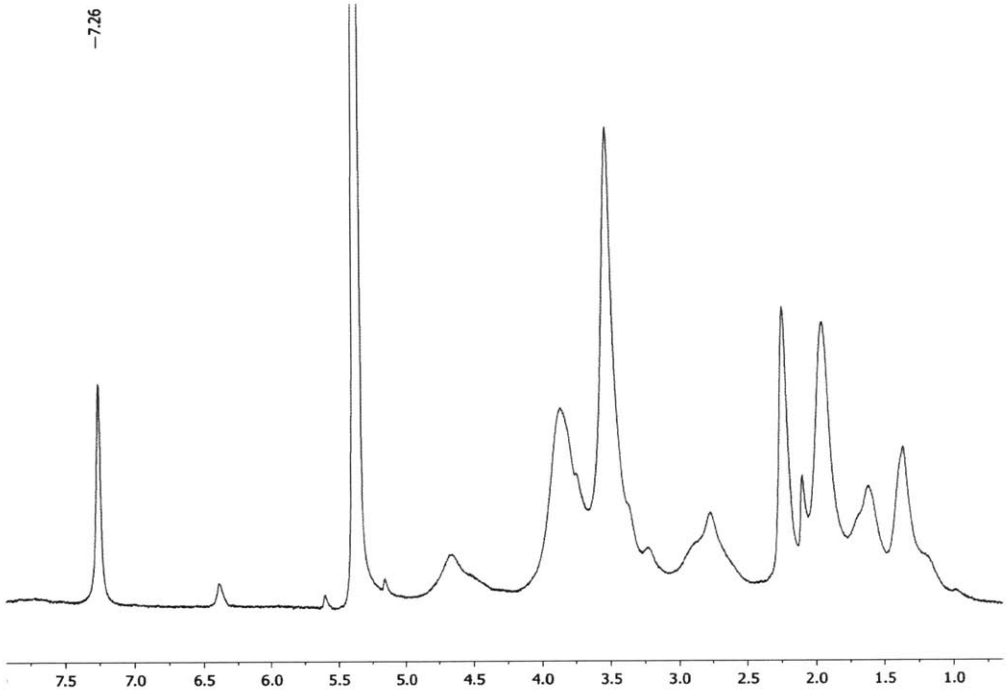

Chex azide. ^{1}H NMR (400 MHz, $CDCl_3$, r.t.) Broad, overlapping signals are expected for radical species.

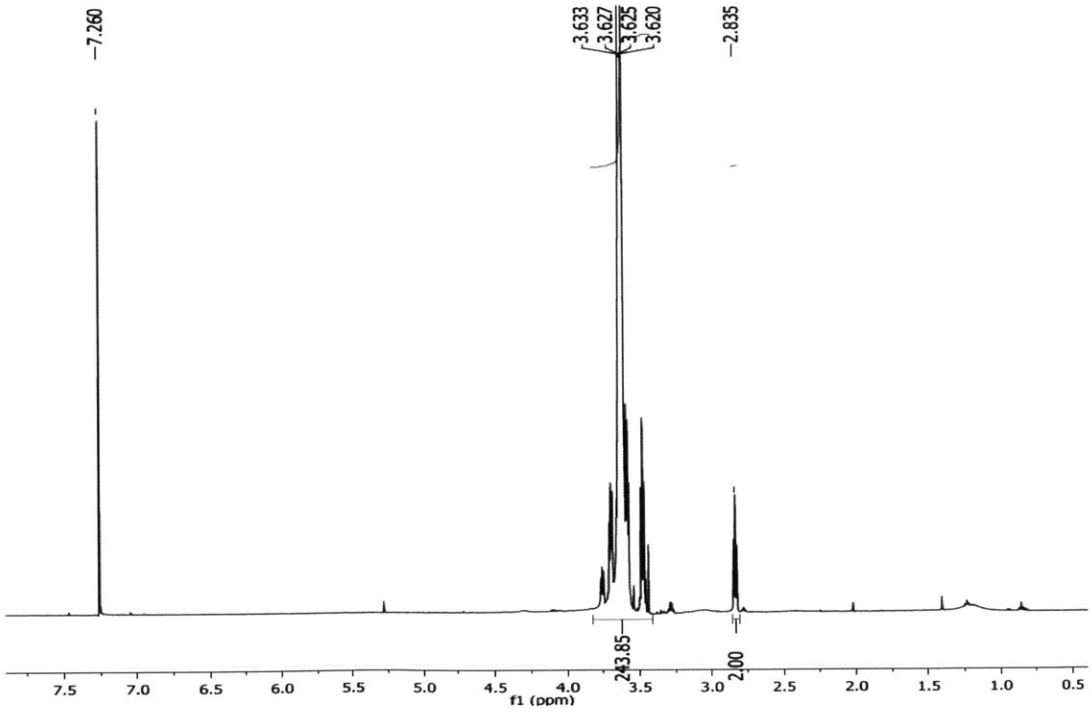

PEG-NH_2. ^{1}H NMR (400 MHz, $CDCl_3$, r.t.)

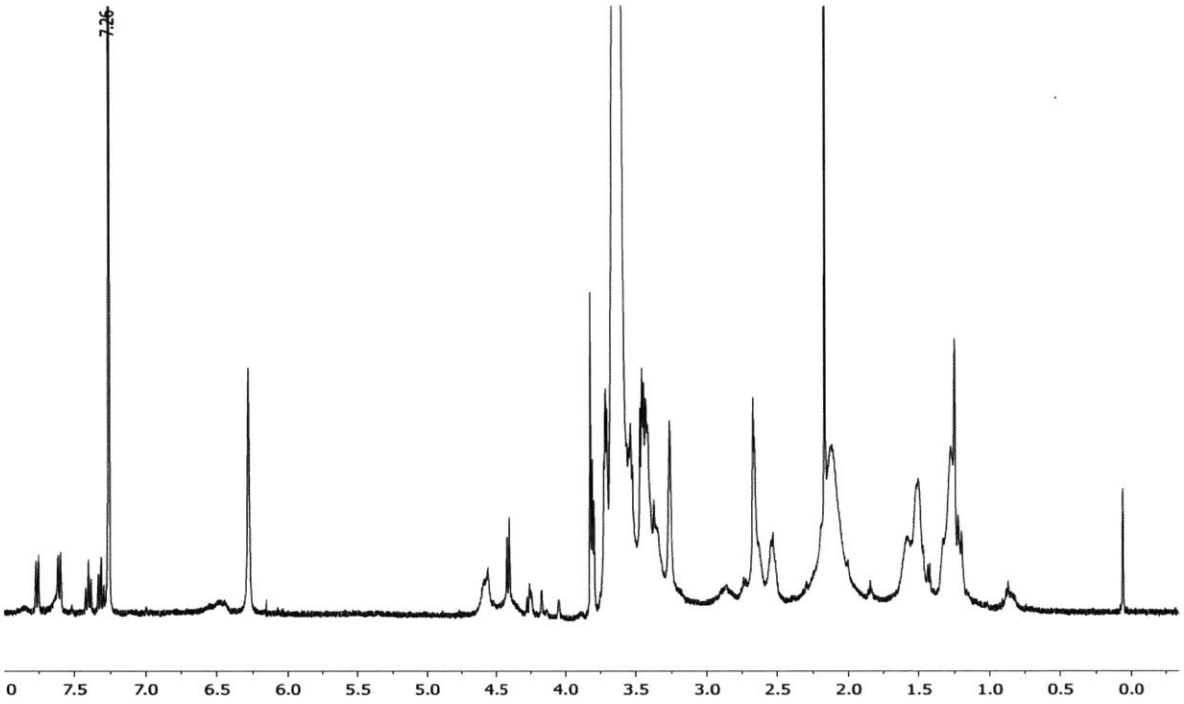

chex-MM ^{1}H NMR (400 MHz, $CDCl_3$, r.t.)

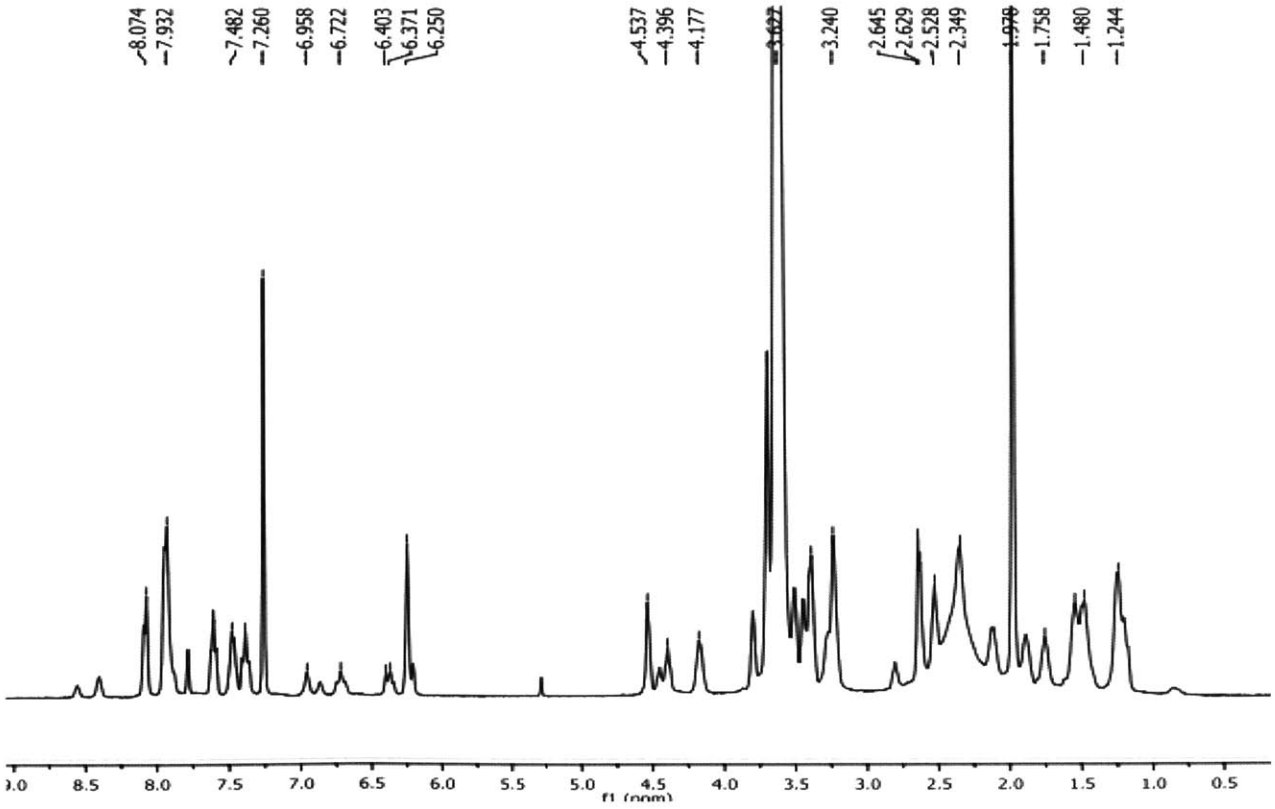

Cy5.5-MM ^{1}H NMR (400 MHz, $CDCl_3$, r.t.)

Chapter 2: Gadolinium-based MRI contrast polymers

Introduction. In addition to the formation of organic MRI contrast agents, we have also explored the area of gadolinium-based bottlebrush polymers. While the fluorescence redox effects described in the previous system would not be applicable, chelated gadolinium contrast agents have a much higher relaxivity than organic radicals.[48] There are several small molecule gadolinium chelates in clinical use, generally focused on T1 weighted MRI. While free gadolinium is highly toxic, these contrast agent chelates are deemed generally safe for adults with functioning kidneys,[50,51] and typically display contrast increases of roughly 50 times the per nitroxide contrast displayed by the previously described ORCAfluors.[52,53]

Studies on polymers,[54-56] dendrimers,[57-60] and other macromolecular systems[61,62] containing multiple Gd^{3+} ions have shown heightened relaxivity per ion due to constructive interactions between closely bound spins.[63] Macromolecular contrast agents have become a very popular field of research, but have not been readily adopted clinically due to several significant drawbacks. Processing of multi-ion imaging agents is plagued by tedious synthesis, poor

Scheme 2. Synthesis of **Gd-MM**.

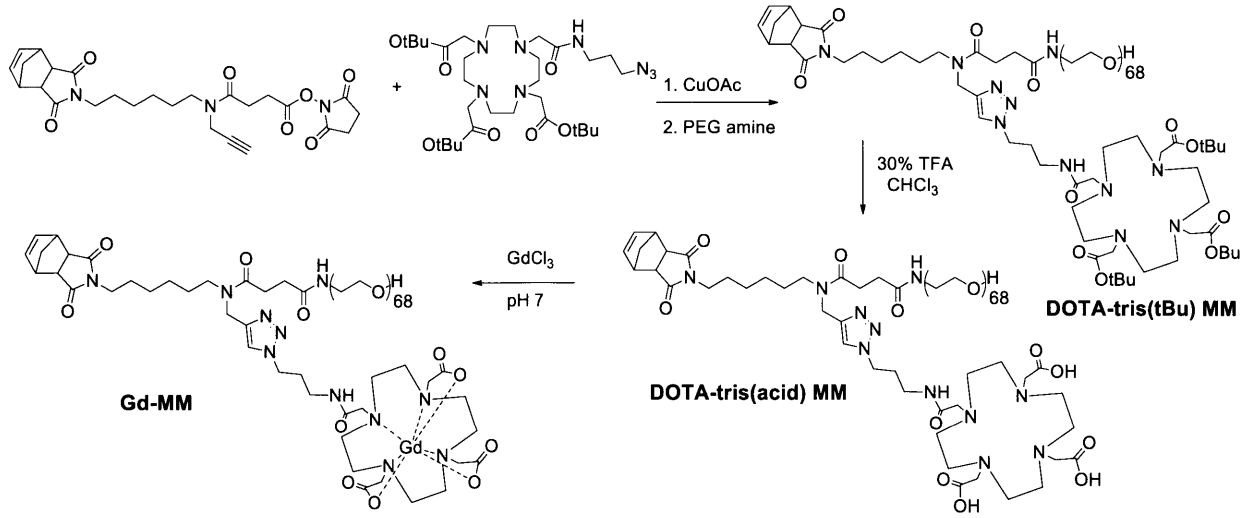

stability, low solubility, or high size variability, while efficacy is mitigated by increased toxicity due to drastically decreased clearance rates.[64]

Synthesis of a gadolinium loaded macromonomer (**Gd-MM**) could alleviate many of these issues. To our knowledge, ROMP of a Gd^{III} tetraazacyclodecane-tetraacetic acid (DOTA) conjugate has not been previously demonstrated. Toward this effect, we have attempted several syntheses, the most promising of which is outlined in Scheme 2. Because gadolinium provides much stronger contrast enhancement than the previously studied nitroxides, a similar magnitude of MRI contrast may be obtained using a decreased concentration of contrast active MM. In this way it would be possible to copolymerize low fractions of MRI-active and fluorescent macromonomers alongside drug loaded or targeting macromonomers to administer effective ratios and doses of multiple functionalities in the same polymer construct. The ability to tag any ROMP polymer with small amounts of MRI-active and fluorescent MMs would allow great flexibility in examining *in vivo* polymer pharmacokinetics.

Results and Discussion. Several routes to the proposed MM were attempted with varying degrees of success. Briefly, the less successful attempts are summarized here.

I. To avoid copper ligation within DOTA, a copper free click strategy was devised using dibenzocyclooctyne (DBCO). *Tert*-butyl protected DOTA azide was clicked to a Nb-*branch*-DBCO NHS ester. The NHS group was displaced using PEG amine. Deprotection of the *tert*-butyl groups proved problematic; NMR analysis suggested decomposition of the MM in 50% TFA/DCM.

II. A similar method to attempt I was explored using non-protected *tris*-acid DOTA azide; however solubility of the non-protected azide limited the reaction conversion.

III. In a third method, aqueous copper sulfate CuAAC conditions were applied to react Nb-*branch*-alkyne PEG3k MM with gadolinium loaded *tris*-acid DOTA azide. Several aqueous conditions were explored to maximize click conversion, but satisfactory conversion was never obtained.

The most successful strategy for MM formation is outlined in Scheme 2. Using the more soluble tBu-protected DOTA azide allowed for more efficient copper acetate/DCM CuAAC conditions. Copper ligation with *tert*-butyl protected DOTA in the CuAAC step necessitated the use of a full equivalent of copper. While not ideal, this complication is not synthesis limiting; DOTA is specifically designed to chelate gadolinium, so any bound copper can be replaced by heating at 80° C with a large excess of $GdCl_3$.[65] Purity of the final **Gd-MM** is difficult to verify; the paramagnetism of Gd^{3+} renders NMR difficult to interpret, MALDI-TOF does not give clean distributions, and HPLC purity is not very trustworthy for PEG-based compounds due to similar elution times. Synthesis of this compound has been performed on small scale and must be scaled up to test polymerization and relaxivity properties.

Conclusions. This chapter describes several synthetic strategies for the synthesis of gadolinium loaded MRI contrast agents based on branched macromonomers. Gadolinium was coordinated using tris-DOTA, a ligand containing three carboxylic acids known to bind Gd^{III} ions orders of magnitude more strongly than Cu^{II} ions. Polymerization of this branched macromonomer remains to be done. Note that the polar gadolinium MM as synthesized was not

readily soluble in standard solvents for ROMP like THF and DCM. However, ROMP in DMF has not been attempted and should be possible. After successful polymerization, this macromonomer will be highly useful for MRI tagging of other ROMP polymers.

Experimental Methods.

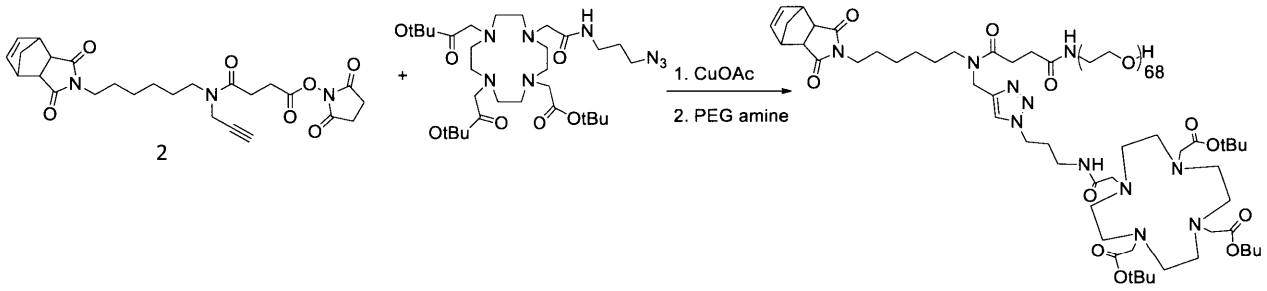

DOTA-tris(tBu) MM. Compound **2** (1.3 mg, 2.6 mmol) was added to a vial with tris-tBu-DOTA propyl azide (Click Chemistry Tools, 2 mg, 2.8 mmol) and 1 mL dry DCM under N_2. A spatula tip of CuOAc was added and the vial was flushed with N_2. After five minutes, LC/MS analysis of the reaction indicated roughly 50% conversion of **2** to the intermediate triazole-*branch*-NHS compound. A second aliquot of CuOAc was added, and the reaction was deemed complete by LC/MS analysis after 15 minutes. Solid PEG-NH_2 (7.7 mg, 2.5 mmol) was then added to the reaction and the mixture was stirred for 14 h. The entire reaction mixture was dried on a rotary evaporator, redissolved in MeOH (0.7 mL), passed through a 0.4 □m Nylon syringe filter, and subjected to prep-HPLC. The pure fractions containing **tBu-DOTA MM** were condensed with a rotary evaporator. The resulting residue was dissolved in dichloromethane (DCM), dried over Na_2SO_4, condensed on a rotary evaporator, and dried overnight under vacuum to yield a pale blue solid in 77% yield. ^{1}H NMR is shown below.

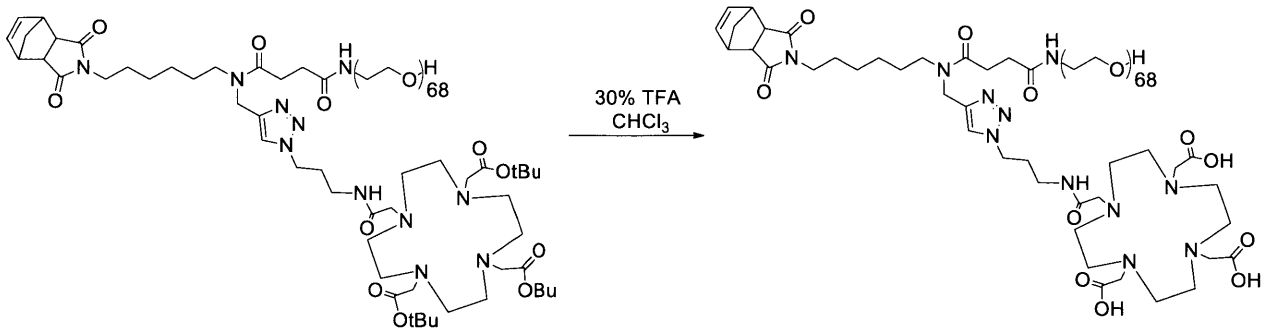

DOTA-tris(acid) MM. tBu-DOTA MM was dissolved in 3 mL of dry chloroform. Trifluoroacetic acid (1 mL) was added, and the reaction was stirred for two hours at room temperature. 5 mL of water was added and the pH was adjusted to 4 with saturated sodium bicarbonate solution, then extracted four times with 20 mL DCM. Extracts were dried over sodium sulfate, condensed on a rotary evaporator, and precipitated into cold diethyl ether. Precipitate was filtered and dried overnight under vacuum, yielding a pale blue powder. ^{1}H NMR is shown below.

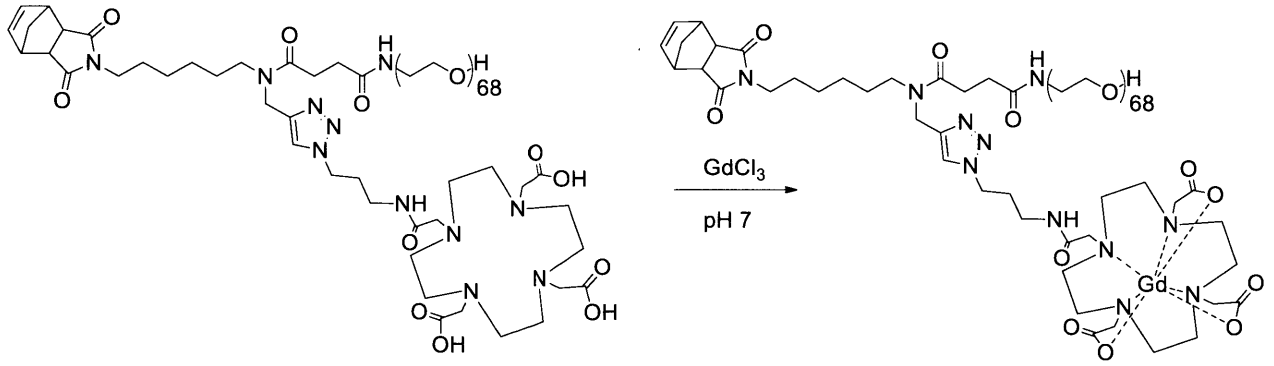

Gd MM. To coordinate gadolinium and displace any bound copper, **DOTA MM** was dissolved in 4 mL of Millipore water along with 20 equivalents of $GdCl_3$. The pH was adjusted to 7 using 1M sodium hydroxide. The reaction was stirred at 70° C for 8 hours, readjusting the pH to 7 every two hours. To remove excess $GdCl_3$, the solution was basified to pH 10 and filtered

through a 0.44 μM syringe filter. The resulting filtrate was extracted four times with 10 mL of DCM. Extracts were dried over sodium sulfate, condensed on a rotary evaporator, and precipitated into cold diethyl ether. Precipitate was filtered and dried overnight under vacuum, resulting in a white powder. Note: this MM was not purified by preparatory HPLC, which would be recommended before ROMP.

Spectral Data.

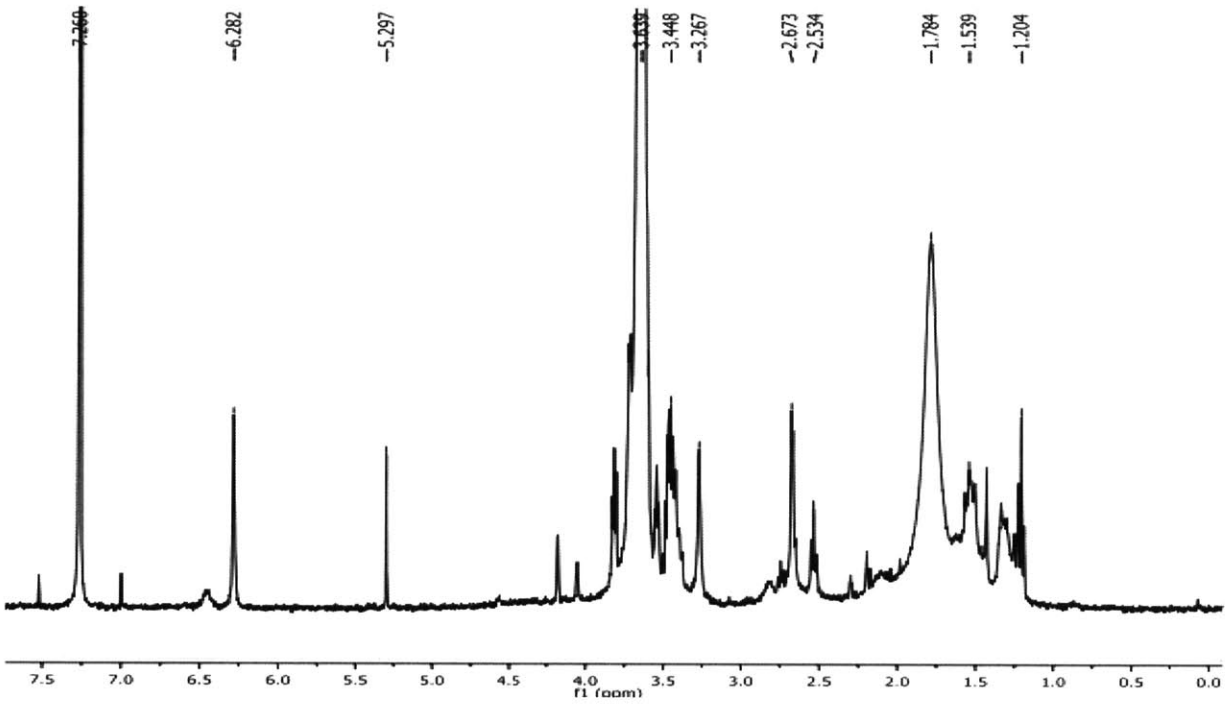

DOTA-tris(tBu) MM ^{1}H NMR (400 MHz, $CDCl_3$, r.t.)

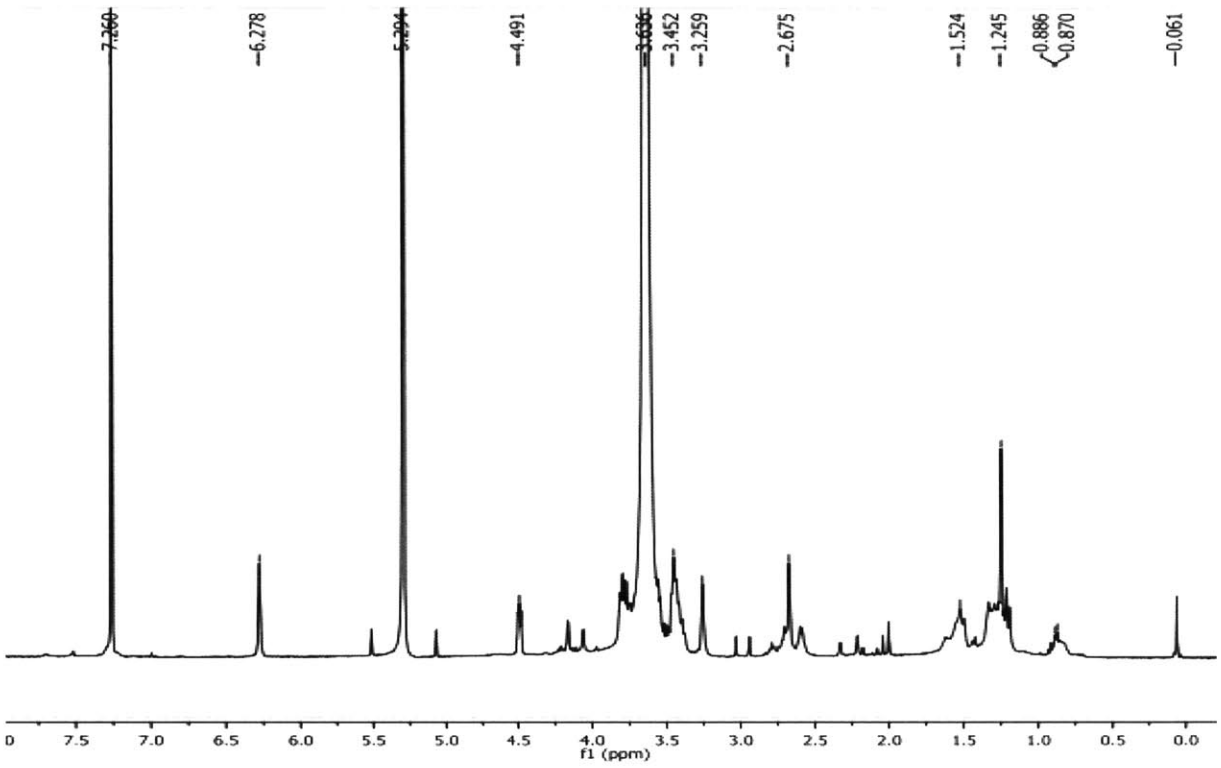

DOTA-tris(acid) MM ^{1}H NMR (400 MHz, $CDCl_3$, r.t.)

Chapter III. Surface functionalization for targeting and cellular internalization

Introduction. A natural extension of the previously described research in polymers for imaging is the incorporation of targeting moieties for tissue/cell-selective imaging. Many previously developed ligands and peptides are known to selectively traffic to tumor cells, including prostate-specific membrane antigen (PSMA),[66-68] RGD peptides,[69,70] and folic acid.[71,72] When combined with the EPR effect,[73,74] active targeting and increased cellular internalization rates could appreciably affect a delivery system's pharmacodyamic and pharmacokinetic

properties.[74,75] In this section, strategies for conjugation of folic acid, as well as the conjugation and synthesis of PSMA, cyclic RGDfK peptide (cRGD), and linear RGD (lRGD) will be discussed. The syntheses of these ligands were conducted according to literature procedures[76,77] using solid phase peptide synthesis and phosgene coupling, respectively.

To maximize the active targeting effect of these ligands, they should be placed on the periphery of a particle,[78] not in the core where previously described MM functionalization has been performed. Furthermore, the ideal MM design would include multiple functionalities to maximize contrast agent and/or drug loading. Conjugation of multiple functionalities necessitates a new approach to the incorporation of targeting ligands. To assure low dispersities and high purity, a highly efficient conjugation technique should be employed. Click chemistry is proven to be efficient in branched macromonomer formation; therefore addition of targeting ligands must be chemically orthogonal to click reactions.

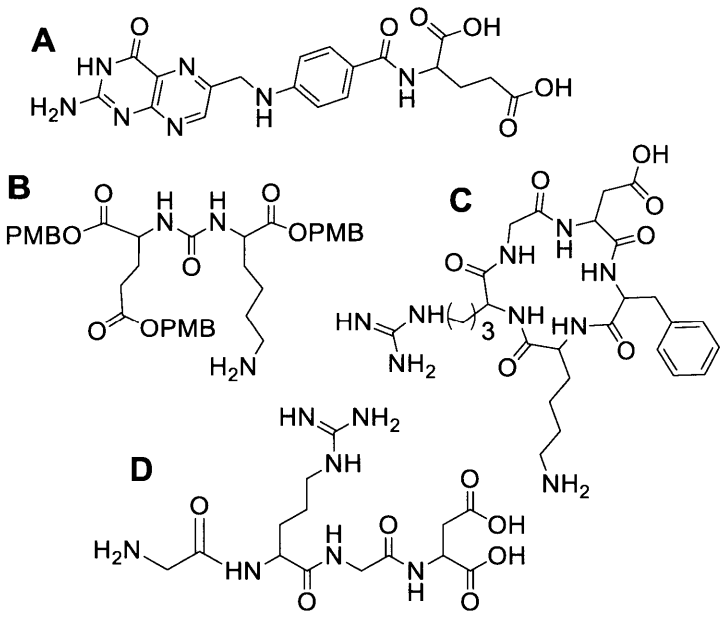

Figure 8. Targeting ligands for PEG conjugation. A. Folic acid **B.** Prostate specific membrane antigen ligand (PSMA) **C.** Cyclic RGD (cRGD) **D.** Linear RGD (lRGD).

Because several of the ligands in question contain lysine residues, two methods of end functionalization of PEG were explored utilizing the primary amine of the lysine side chain. Our first option was an amide coupling reaction with a carboxylic acid terminated PEG. When complete conversion to carboxy PEG proved difficult, a second route was developed. The free

amine sidechain of lysine could be used as an S_N2 nucleophile to react with mesylated PEG. This method results in a secondary amine, which is not amenable to ROMP with most Grubbs' catalysts; however, pseudo-protection of the amine as an ammonium should allow for polymerization to proceed. Described here are the positive and negative results from these trials, with the most promising data arising from S_N2 and subsequent quaternization.

Results and Discussion. Solid phase peptide synthesis (SPPS) was utilized to create linear GRGD and RGDfK peptides. A scheme for this synthesis can be found in the experimental methods section. Briefly, using Fmoc/Boc protected peptides and HBTU/HOBt coupling conditions, these peptides were cleaved from resin and purified via HPLC. The pentapeptide was cyclized using propylphosphonic anhydride (T3P), and purified using column chromatography.[76]

PSMA was made via paramethoxybenzyl protection of carboxylic acids on glutamic acid and Fmoc-Lys(Boc). The Fmoc-lysine amine was deprotected in 20% piperidine, and the amino acids were coupled using triphosgene. The fully protected product was purified by flash chromatography.[77] Schemes for this synthesis are found in the preceeding experimental methods section.

Several oxidation methods were attempted for converting the PEG terminal alcohol to a carboxylic acid. First, PEG 3000 monoamine was protected using fluorenylmethyloxycarbonyl (Fmoc) chloride. A second portion of PEG monoamine was reacted with norbornene-glycine-NHS ester, yielding **PEG MM**. These PEG monoalcohols were oxidized using several different Jones oxidation conditions summarized in Table 2, as well as TEMPO/cyanuric acid oxidation. When none of these oxidation techniques provided high yields and/or conversions, a second method of conversion to carboxylic acid was attempted.

Starting Material	CrO_3 (eq.)	Acetone (%)	H_2O (%)	H_2SO_4 (eq.)	Conditions
2k Fmoc PEG	3	50	50	9	3h, 0 → r.t.
2k Fmoc PEG	3	0	100	50	24h, r.t.
2k MM	1.2	50	50	50	14h, r.t.
2k MM	0.9	0	100	20	24h, r.t.
3.2k MM	6	0	100	20	24h, r.t.
3.2k MM	6	0	100	100	24h, r.t.

Table 3. Jones oxidation conditions. A list of attempted Jones oxidations is provided. None of the above conditions provided acceptable yield and/or conversion on scales of >30 mg of starting material

In 2011, Pichavant et al reported a method of carboxylating alcohol terminated PEG for conjugation of antibiotics to ROMP polymers.[79] Following their procedure, ethyl bromoacetate was added to PEG monoalcohol to afford an ethyl ester MM. This ester was hydrolyzed overnight in 4M NaOH. Conversions during this sequence of reactions were very high; however, an appreciable amount of final neutralized product was lost during isolation. While this appeared to be the most effective route toward carboxylation, nucleophilic attack of a PEG mesylate was attempted before further coupling studies were performed.

To test the S_N2 reactivity of **Mesyl MM**, pilot studies were performed using benzylamine as the nucleophile. Scheme 3 outlines this synthesis, beginning with the mesylation of **PEG-MM**. This mesylated product (**Mesyl MM**) was added to a large excess of amine and stirred at room temperature overnight. The resulting secondary amine was quaternized using either methyl iodide or hydrochloric acid before isolation. Polymerization of these cationic monomers was achieved in quantitative yield, providing proof of principle for this charged construct. In addition

Scheme 3. S_N2 synthesis of cationic MM. Sequential mesylation and displacement with an amine demonstrates one possible end functionalization of PEG macromonomers.

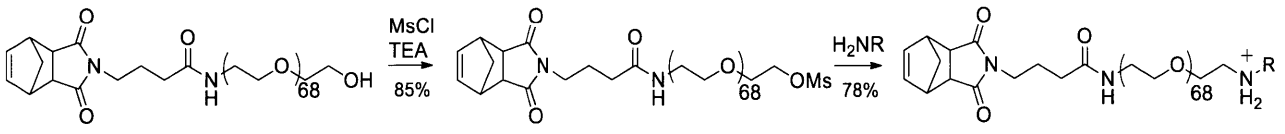

PEG MM **Mesyl MM** **Cationic MM**

to more efficient synthesis and higher yields, addition of charge to targeting MMs may provide increased cellular internalization, a property common amongst polycationic polymers.[80,81]

Bottlebrush polymers made from cationic MMs had slightly larger hydrodynamic radii than the equivalent non-charged MM of the same molar mass. This indicates that PEG chains are more extended in the cationic construct, likely due to charge-charge interactions between chain ends. High surface charge has been show to vastly increase cellular uptake rates; polyarginines and polylysines are commonly added to drug carriers to increase efficacy.[82-85] Similarly, higher charge concentration on the shell of the nanoparticle prompts the possibility of layer-by-layer and ionic assembly interactions.[86,87]

Previous studies of hyaluronic acid have shown selective targeting to triple negative breast cancer cells.[7,88] To demonstrate the potential to assemble non-covalent shell-core nanoparticles, hyaluronic acid (10kDa MW) was added to a solution of 50 unit cationic bottlebrush polymer. Nanoparticles were stirred overnight at room temperature, then filtered through a 0.44 μM nylon syringe filter. The hydrodynamic diameters before and after ionic coordination were 19.0 nm and 26.0 nm respectively (Figure 9), a 37% diameter increase. Further TEM and zeta potential analysis will be necessary to confirm addition of a negatively charged polymer layer.

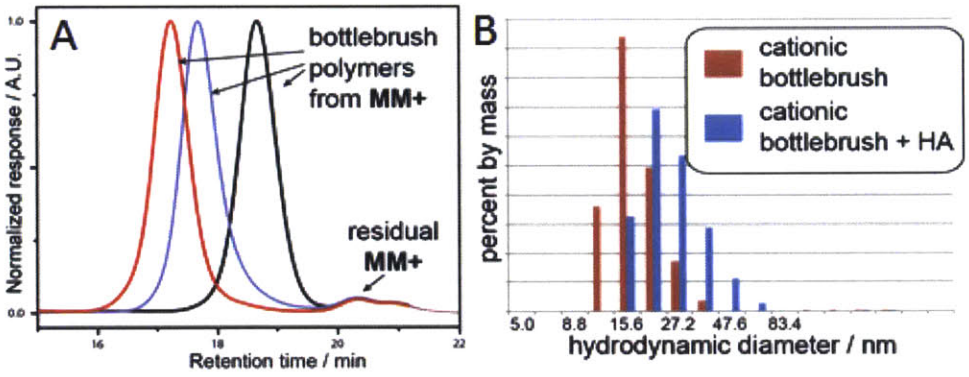

Figure 9. Cationic MM formation and coordination of hyaluronic acid. **A.** GPC traces of 10, 50, and 100 unit brushes composed of cationic MMs. **B.** DLS characterization of a 50 unit cationic MM brush before and after coordination with poly anionic hyaluronic acid.

Folic acid is another common ligand used to target the upregulated folate receptors on cancer cells.[72,89]. PEG 2000 bisamine was synthesized from PEG diol via mesylation and displacement with 38% aqueous ammonia. An active folate NHS ester was synthesized with dicyclohexylcarboimide (DCC) in DMSO according to literature procedures.[90] After purification by trituration in cold ether, the folate-NHS was added to PEG bisamine in a one-to-one ratio. Due to the highly polar nature of folic acid, statistical bis-, mono-, and non-reacted products can be easily separated by HPLC. The remaining amine was used to displace norbornene-NHS, yielding a linear folic acid MM. The solubility of this MM was very low in all solvents other than DMSO and DMF, which is unexpected and could indicate that the MM was impure. Trial polymerizations in 20, 50, and 100% DMSO were unsuccessful; DMF remains a possibility.

Conclusions. This chapter describes the synthesis of several targeting moieties, alongside the synthesis, characterization, and polymerization of several cationic macromonomers. These surface and end functionalities can be used in combination with previously described imaging or drug loaded macromonomers for selective delivery of nanoparticle payload. Coordination of cationic polymer brushes with hyaluronic acid provides first evidence for the use of this macromonomer motif for non-covalent multi-layer nanoparticle assembly. The high cationic content of the outer layer of these charged bottlebrush polymers provide opportunity for increased cellular uptake rates.

Experimental Methods.

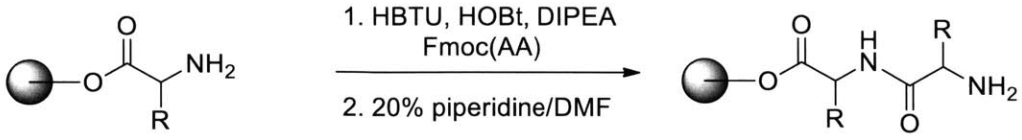

SPPS of peptides. A general procedure for peptide coupling is described below. 2-Chlorotrityl glycine resin (0.193 g (0.46 mmol/g loading), 0.089 mmol) was added to a peptide synthesis flask and swollen in DCM for 30 minutes. Resin was washed twice with DMF (10 minutes while agitating with air). The next amino acid in the sequence (0.267 mmol) was added to a vial with HBTU (0.267 mmol, 101 mg), HOBt (0.267 mmol, 41 mg), *N,N*-diisopropylethylamine (0.534 mmol, 0.093 mL), and 5 mL DMF. The reaction was stirred for 10 minutes, then added to the resin and agitated with air for 2 hours. A Kaiser test was performed to determine reaction completion. Once complete, DMF was drained and the resin was washed three times with 20 mL DMF.

A solution of 20% piperidine in DMF (10 mL) was added to the synthesis flask and agitated for 30 minutes. Resin was washed again with DMF, and the procedure was repeated to add subsequent residues.

To cleave peptide from resin, 1% TFA in DCM (10 mL) was added to the flask and agitated for 10 minutes. 2 mL of 10% pyridine in methanol was added to a collection flask to neutralize the TFA upon draining the synthesis flask. This was repeated five times, DMF was removed with a rotary evaporator and the peptide was purified by HPLC.

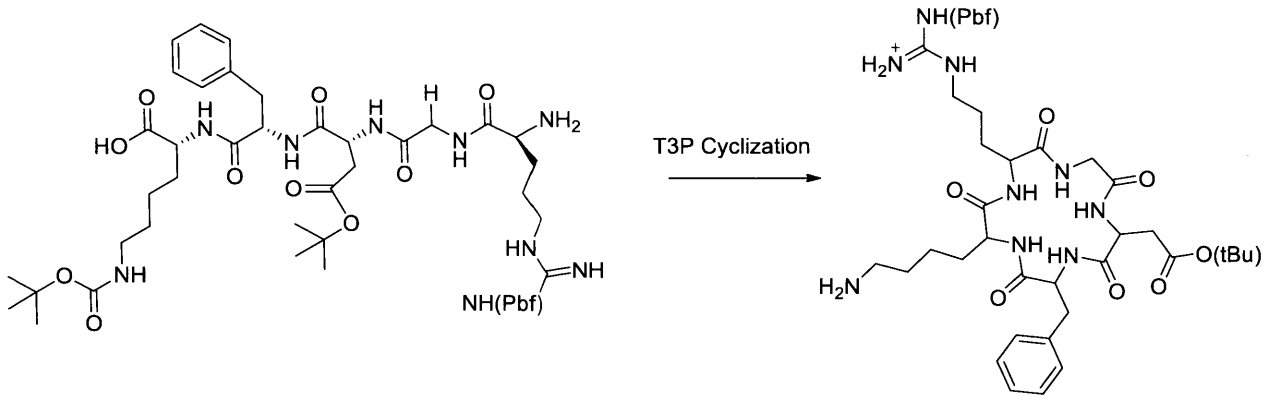

T3P cyclization of cRGD. In a 250 mL flask, T3P (1.5 mL, 100 mmol) and DIPEA (1 mL, 200 mmol) were added along with 100 mL DMF. Linear pentapeptide (210 mg, 4.9 mmol) was dissolved in 20 mL DMF and added slowly via addition funnel and stirred overnight at room temperature. The ^{1}H and ^{13}C NMR spectra are shown in the following section. MS calcd. for $C_{44}H_{66}N_9O_{10}S^+$ $[M+H]^+$, 912.465; found 912.3.

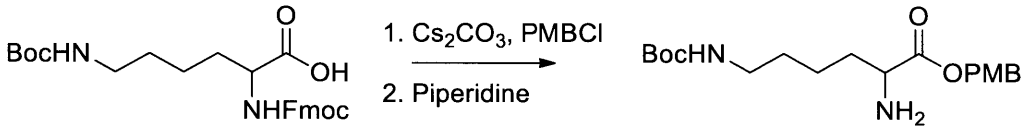

Lys(Boc) PMB. Fmoc Lys(Boc) (5.44 g, 11 mmol) and cesium carbonate (5.3 g, 16 mmol) were added to a 100 mL flask which was evacuated and refilled three times. Anhydrous DMF (45 mL) was added to the flask, followed by paramethoxybenzyl chloride (1.73 mL, 12 mmol). The reaction was stirred at room temperature for four hours, filtered, and washed with ethyl acetate. In a separatory funnel, ethyl acetate layer was washed with saturated sodium bicarbonate, then with brine. Organic layer was dried over sodium sulfate, condensed on a rotary evaporator, and recrystallized from 60/40 hexanes/ethyl acetate to provide 6.02 g (88% yield) white crystals.

These crystals were dissolved in 50 mL of 20% piperidine in DMF and stirred at room temperature for two hours. The reaction was diluted with 100 mL of brine and extracted three

ties with ethyl acetate. The organic fraction was washed with brine, condensed on a rotary evaporator to provide a white solid. The product was purified using flash chromatography to afford a colorless oil in 83% yield. The ^{1}H and ^{13}C NMR spectra are shown in the following section.

^{1}H NMR (400 MHz, $CDCl_3$) δ 1.35 (m, 2H), 1.45 (s, 9H), 1.51-1.73 (m, 6H), 3.06 (t, 2H), 3.41 (t, 1H), 3.80 (s, 3H), 4.52 (br. s, 1H), 5.07 (s, 2H), 6.88 (d, 2H), 7.27 (d, 2H). ^{13}C NMR (400 MHz, $CDCl_3$) δ 22.79, 28.40, 29.73, 31.41, 34.34, 36.46, 40.29, 53.44, 54.34, 55.26, 64.68, 66.47, 79.02, 113.90, 127.81, 128.53, 130.18, 155.99, 159.72, 162.18, 175.87. MS calcd. for $C_{19}H_{30}N_2O_5$ $[M+H]^+$, 367.223; found 367.2.

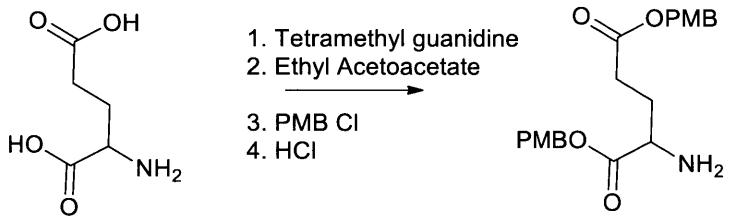

Glu(PMB_2). Glutamic acid (0.117 g, 0.8 mmol) was suspended in dry DMF under an N_2 atmosphere and cooled in an ice bath. Tetramethylguanidine (0.2 mL, 1.6 mmol) was added and stirred at room temperature for 30 minutes. Ethyl acetoacetate (0.1 mL, 0.8 mmol) was added and the reaction was continued to stir for 3 hours until completely dissolved. PMB chloride (0.22 mL, 1.6 mmol) was added, and the reaction was stirred for 24 hours. A white had formed at this point, and the reaction was diluted with ethyl acetate and extracted with saturated sodium bicarbonate. Hydrolysis in 2 mL of 1.25 M methanolic HCl was performed, and the reaction was condensed to a white powder which was subsequently recrystallized in ethyl acetate affording

283 mg (84% yield) colorless crystals. The ^{1}H and ^{13}C NMR spectra are shown in the following section.

^{1}H NMR (400 MHz, $CDCl_3$) δ 2.38 (m, 2H), 2.56 (m, 2H), 3.75 (s, 6H), 4.29 (br. s, 1H), 4.95 (s, 2H), 5.08 (t, 2H), 6.80 (d, 4H), 7.23 (d, 4H), 8.90 (br. s, 2.75H). ^{13}C NMR (400 MHz, $CDCl_3$) δ 25.35, 29.86, 52.55, 55.22, 66.44, 68.16, 113.90, 126.66, 127.78, 130.07, 130.40, 159.57, 159.86, 172.25. MS calcd. for $C_{21}H_{25}NO_6$ $[M+H]^+$, 388.175; found 388.3.

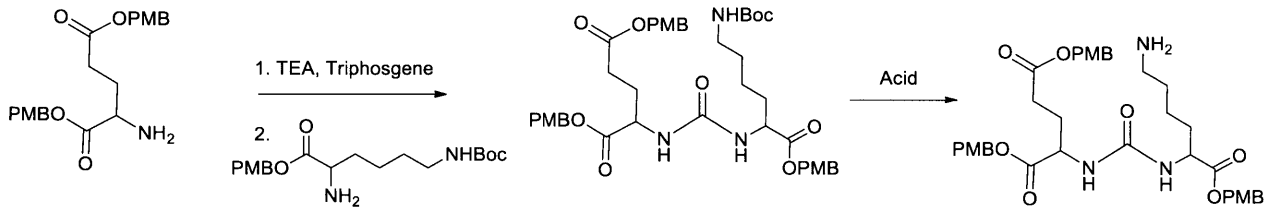

Boc-PMSA-PMB$_3$. In a vial under inert atmosphere, glutamic acid(PMB)$_2$ (0.655 g, 1.5 mmol) was dissolved in 4 mL anhydrous DCM. In a second vial, triphosgene (0.153 g, 0.5 mmol) was dissolved in 2 mL DCM. Solutions were combined and cooled to -78° C. Triethylamine (2.15 mL, 15 mmol) was added dropwise, and the reaction was allowed to stir at -78° C for 30 minutes, then warmed to room temperature and stirred for 30 minutes longer. Protected lysine was dissolved in 2 mL dry DCM, added to the reaction, and stirred overnight at room temperature. The product was purified using flash chromatography in 20% ethyl acetate in hexanes affording 0.830 g of white solid (68% yield). The ^{1}H and ^{13}C NMR spectra are shown in the following section.

^{1}H NMR (400 MHz, $CDCl_3$) δ 1.26 (m, 2H), 1.42 (s, 9H), 1.55 (m, 1H), 1.74 (m, 1H), 1.92 (m, 1.2H), 2.17 (m, 1.3H), 2.36 (m, 2H), 3.01 (br. s, 2H), 3.79 (s, 9H), 4.49 (m, 2H), 5.05 (quintet, 6H), 6.85 (m, 4H), 7.25 (m, 6H). ^{13}C NMR (400 MHz, $CDCl_3$) δ 22.30, 27.96, 29.39, 40.08,

52.53, 55.27, 66.26, 67.10, 113.96, 127.59, 130.12, 156.90, 159.61, 173.90, 173.29. MS calcd. for $C_{41}H_{53}N_3O_{12}$ $[M+H]^+$, 780.37; found 780.1.

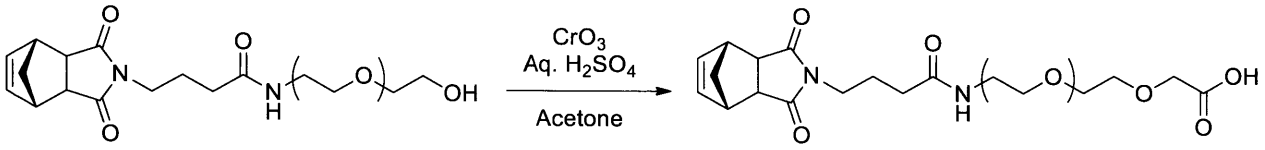

Jones oxidation. A general procedure was followed for all Jones oxidations, with varying amounts of each reagent. Conditions for these trials can be found in Table 2. In general, PEG was dissolved in acetone and cooled on an ice bath. In a separate vial, CrO_3, sulfuric acid, and water were combined and added dropwise to PEG solution, still on ice. The solution quickly turned bright orange and was allowed to warm to room temperature and react open to air. The reaction was quenched with isopropanol, pH was adjusted to 3 with sodium bicarbonate, and PEG was extracted into DCM, condensed on a rotary evaporator, and precipitated into ether.

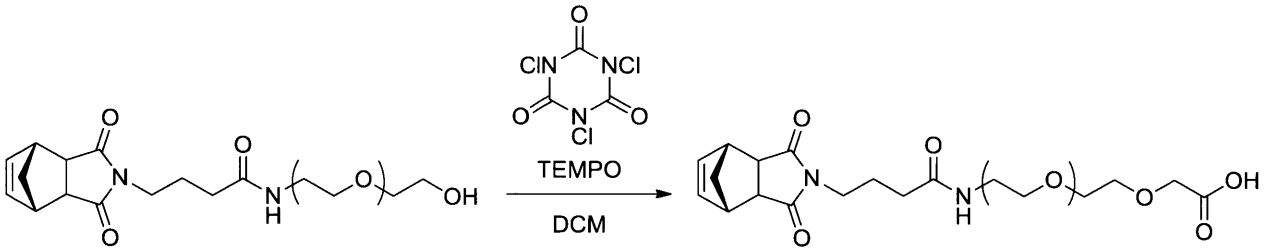

TEMPO oxidation. PEG macromonomer (230 mg, 0.1 mmol) was dissolved in 4 mL acetone and 0.5 mL 15% $NaHCO_3$ and cooled on an ice bath. Sodium bromide (2 mg, 0.02 mmol) and TEMPO (2 mg, 0.01 mmol) were added, followed by slow addition of trichloroisocyanuric acid (48 mg, 0.2 mmol). The reaction was was allowed to warm to room temperature, and monitored by LCMS. Incomplete conversion was shown by LCMS after 24 hours, so reaction was filtered and precipitated into cold ether, obtaining 98 mg (42% yield) of partially oxidized material.

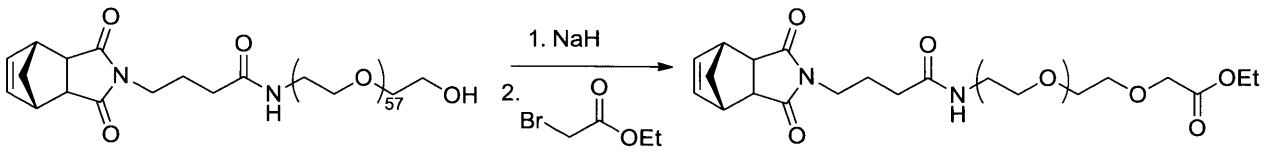

Ethyl bromo acetate. Sodium hydride (8 mg, 0.3 mmol) was washed with three aliquots of hexanes, then dried under vacuum for 20 minutes and suspended in 0.5 mL anhydrous THF. In a separate vial, dry PEG 2000 MM (80 mg, 0.03 mmol) was dissolved in 1 mL THF and transferred to the base solution. The reaction was stirred at room temperature for thirty minutes. Ethyl bromoacetate (26 mg, 0.14 mmol) was added slowly, and the reaction was heated to 60° C and stirred overnight. The reaction was quenched with 10 mL water, then extracted three times with 50 mL DCM, dried over Na_2SO_4, concentrated, and precipitated into cold ether. The resulting white powder was dried under vacuum, providing 67 mg (84% yield) product.

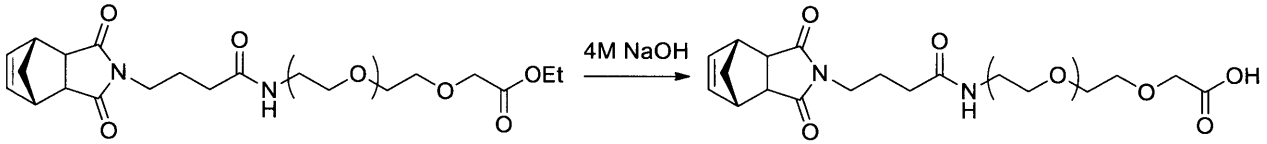

Ester hydrolysis. Ethyl ester MM (67 mg, 0.03 mmol) was dissolved in 4 mL of 1M aqueous NaOH and stirred overnight at 55° C. Water was removed using a rotary evaporator, and the resulting white residue was dissolved in DCM, dried over Na_2SO_4, and precipitated into cold ether providing 32 mg (48% yield) of white powdery solid.

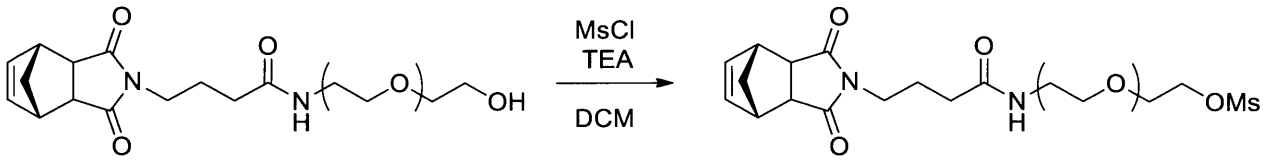

Mesyl MM. PEG MM (304 mg, 0.07 mmol) was added to a vial which was evacuated and refilled three times. Triethylamine (15 mg, 0.15 mmol) and 1 mL of dry DCM were added and

cooled to 0° C. In a separate evacuated and refilled vial, 1 mL dry DCM and mesyl chloride (43 mg, 0.4 mmol) were combined, then added dropwise to the chilled vial of MM. The reaction was allowed to proceed for two hours at 0° C, then condensed on a rotary evaporator, precipitated three times from cold ether, and the white powder was dried under vacuum providing 260 mg product (85% yield). The ^{1}H NMR and MALDI spectra are shown in the following section. MALDI calcd. for $C_{134}H_{258}N_2O_{65}NaS$ $[M+Na]^+$, 2992.511; found 2993.7325.

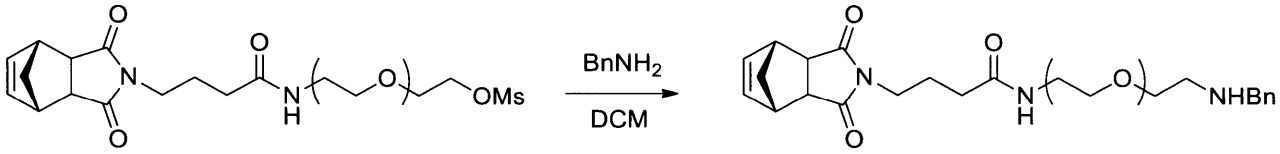

Benzyl MM. Mesyl MM (0.145 g, 0.035 mmol) dissolved in 0.5 mL of dry DMF was added dropwise to 1.5 mL of benzylamine and stirred overnight. The reaction was precipitated four times into cold ether, and the resulting white powder was dried under vacuum yielding 98 mg of product (67%). The ^{1}H NMR and MALDI spectra are shown in the following section. MALDI calcd. for $C_{136}H_{256}N_3O_{60}Na$ $[M+Na]^+$, 2915.699; found 2915.89.

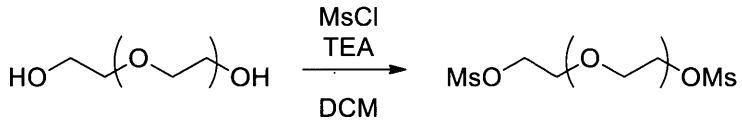

Bismesylate. PEG 2000 diol (3.1g, 1.5 mmol) was added to a vial which was evacuated and refilled three times. Triethylamine (1.1 mL, 7.5 mmol) and 5 mL of dry DCM were added and cooled to 0° C. In a separate evacuated and refilled vial, 2 mL dry DCM and mesyl chloride (0.54 mL, 7 mmol) were combined, then added dropwise to the chilled vial of MM. The reaction was allowed to proceed for two hours at 0° C, then condensed on a rotary evaporator, precipitated three times from cold ether, and the white powder was dried under vacuum

providing 2.7 mg product (87% yield). The ^{1}H NMR and MALDI spectra are shown in the following section. MALDI calcd. for $C_{92}H_{186}O_{50}NaS_2$ $[M+Na]^+$, 2178.135; found 2178.98.

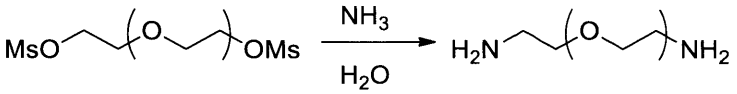

Bisamine. Dry bismesylate PEG (350 mg, 0.16 mmol) was added to a vial with stirbar. 15 mL of 38% aqueous ammonia was added to the PEG and stirred overnight. The reaction was extracted 4 times with DCM. Organic extracts were dried with sodium sulfate, condensed on a rotary evaporator, precipitated three times from cold ether, and the white powder was dried under vacuum, providing 244 mg (70% yield) of product. The ^{1}H NMR and MALDI spectra are shown in the following section. MALDI calcd. for $C_{96}H_{196}N_2O_{47}Na$ $[M+Na]^+$, 2153.294; found 2153.99.

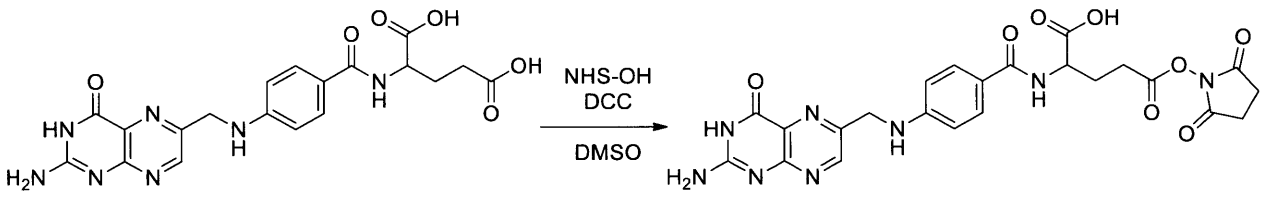

Folic acid NHS. Folic acid (0.5 g, 1.1 mmol), *N*-hydroxysuccinimide (261 mg, 2.2 mmol), and dicyclohexylcarboimide (467 mg, 2.2 mmol) were combined and dissolved in 10 mL DMSO. The reaction was stirred at room temperature overnight in the dark, then filtered through 0.44 μM nylon filter paper and precipitated from room temperature ether 3 times. The resulting orange, gummy solid was triturated in cold ether to obtain 0.357 g (71% yield) fine orange powder. ^{1}H NMR (400 MHz, $CDCl_3$) δ 3.43 (t, 2H), 3.62 (t, 1H), 4.71 (t, 2H), 4.94 (q, 2H), 5.08 (s, 2H), 5.16 (s, 4H), 9.30 (d, 2H), 10.13 (d, 2H), 11.06 (s, 1H). MS calcd. for $C_{23}H_{21}N_8O_8$ $[M-H]^-$, 537.148; found 537.2.

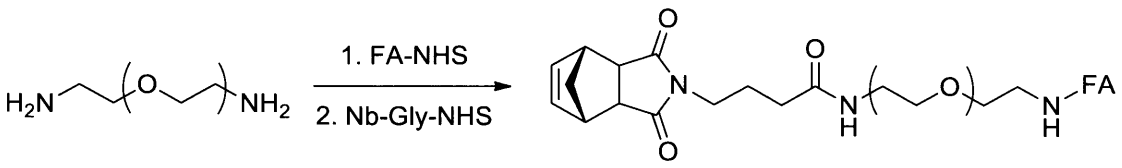

Folic acid MM. PEG bisamine was dissolved in dry DMF. Folic acid NHS was added and stirred 24 hours. Norbornene-glycine-NHS was then added and stirred overnight. The reaction was precipitated, the yellow solid was dissolved in methanol, then filtered through a 0.44 μM nylon syringe filter. The reaction was HPLC purified to separate the desired product from any bis-norbornene and bis-folate PEG. HPLC fractions containing pure product were combined and condensed on a rotary evaporator. DCM was added, and any remaining water was removed using sodium sulfate. Solvent was removed with a rotary evaporator, precipitated from cold ether, and dried under vacuum yielding a yellow solid. The ^{1}H NMR spectrum is shown in the following section.

Spectral Data.

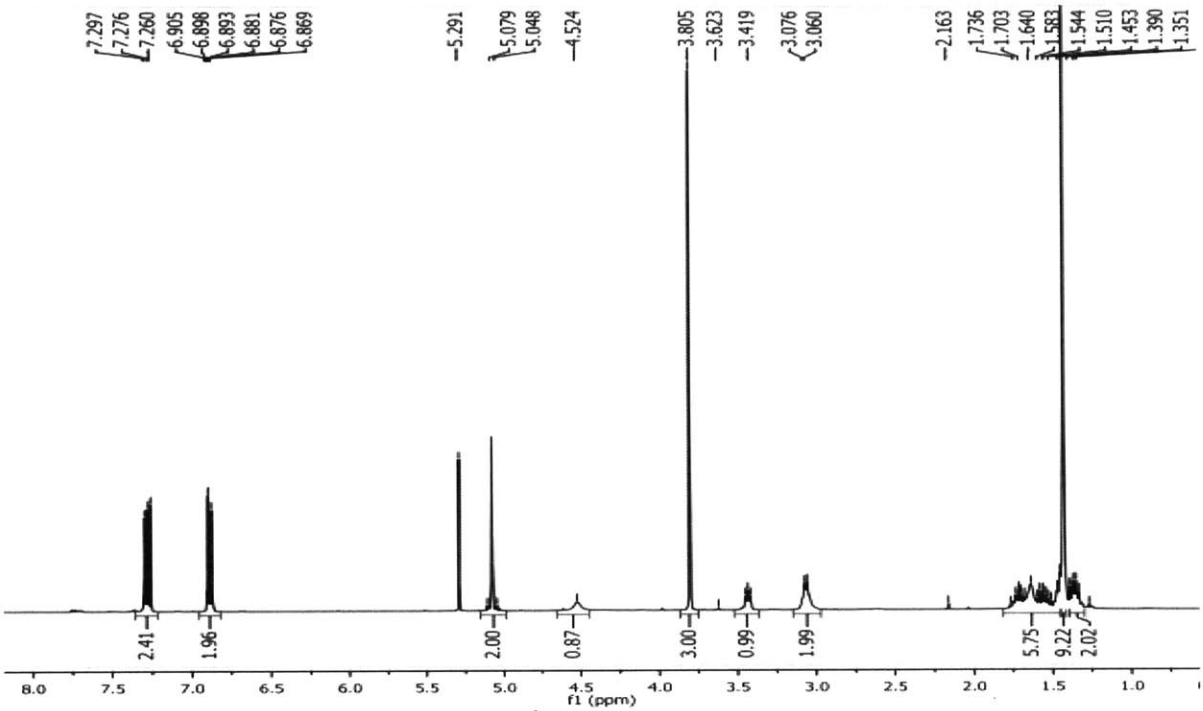

Lys(Boc) PMB ^{1}H NMR (400 MHz, $CDCl_3$, r.t.)

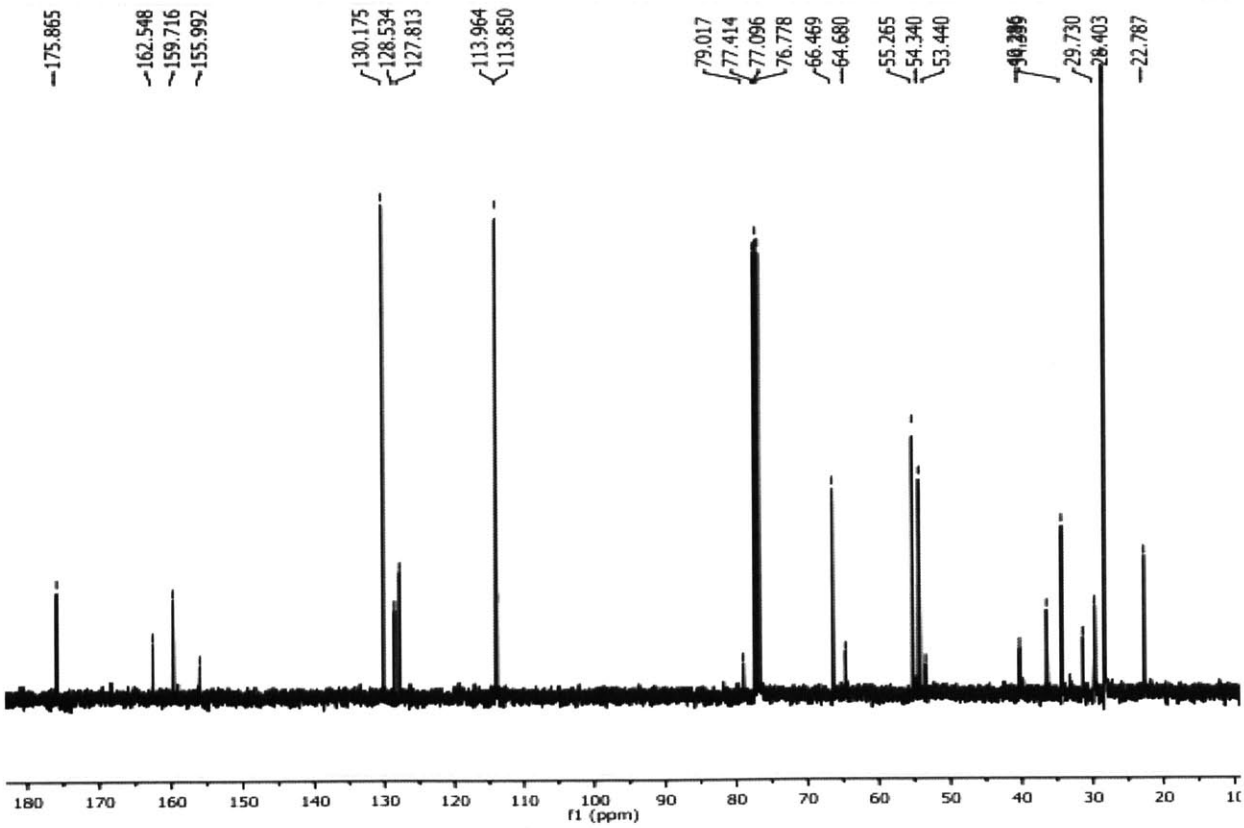

Lys(Boc) PMB ^{13}C NMR (400 MHz, $CDCl_3$, r.t.)

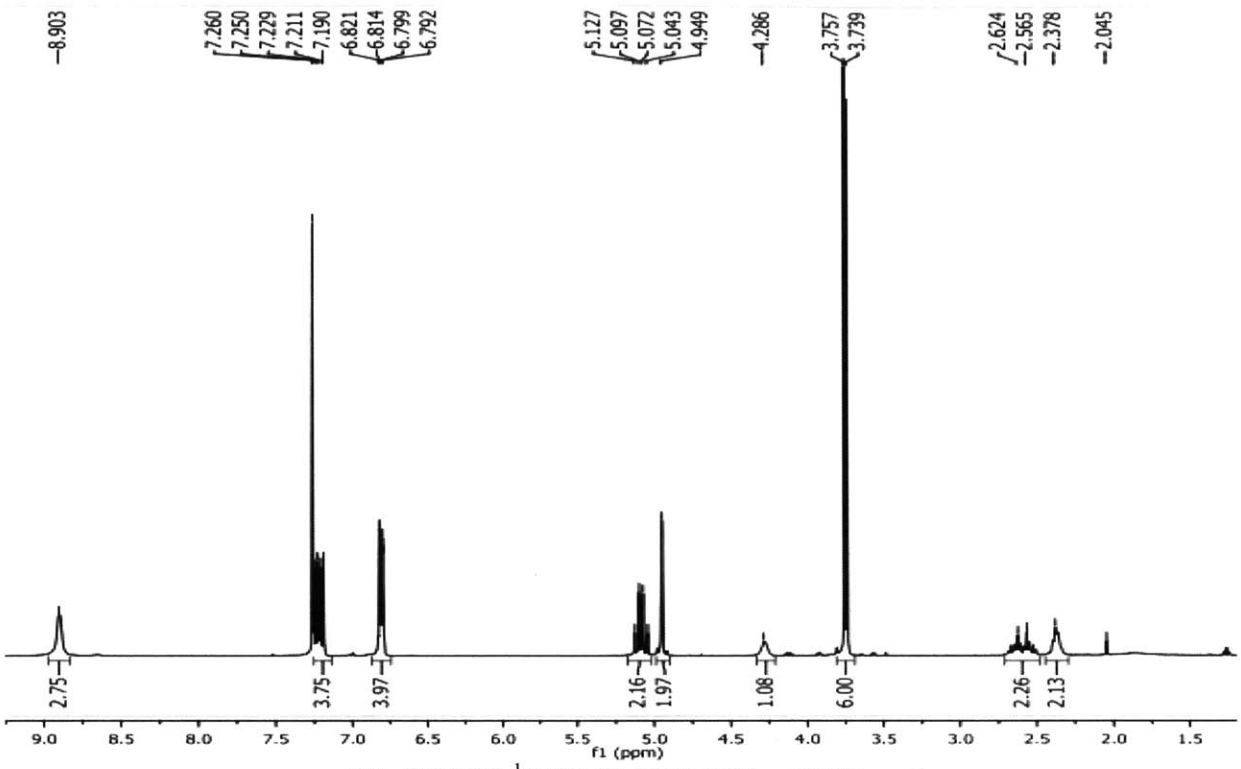

Glu(PMB$_2$) ^{1}H NMR (400 MHz, $CDCl_3$, r.t)

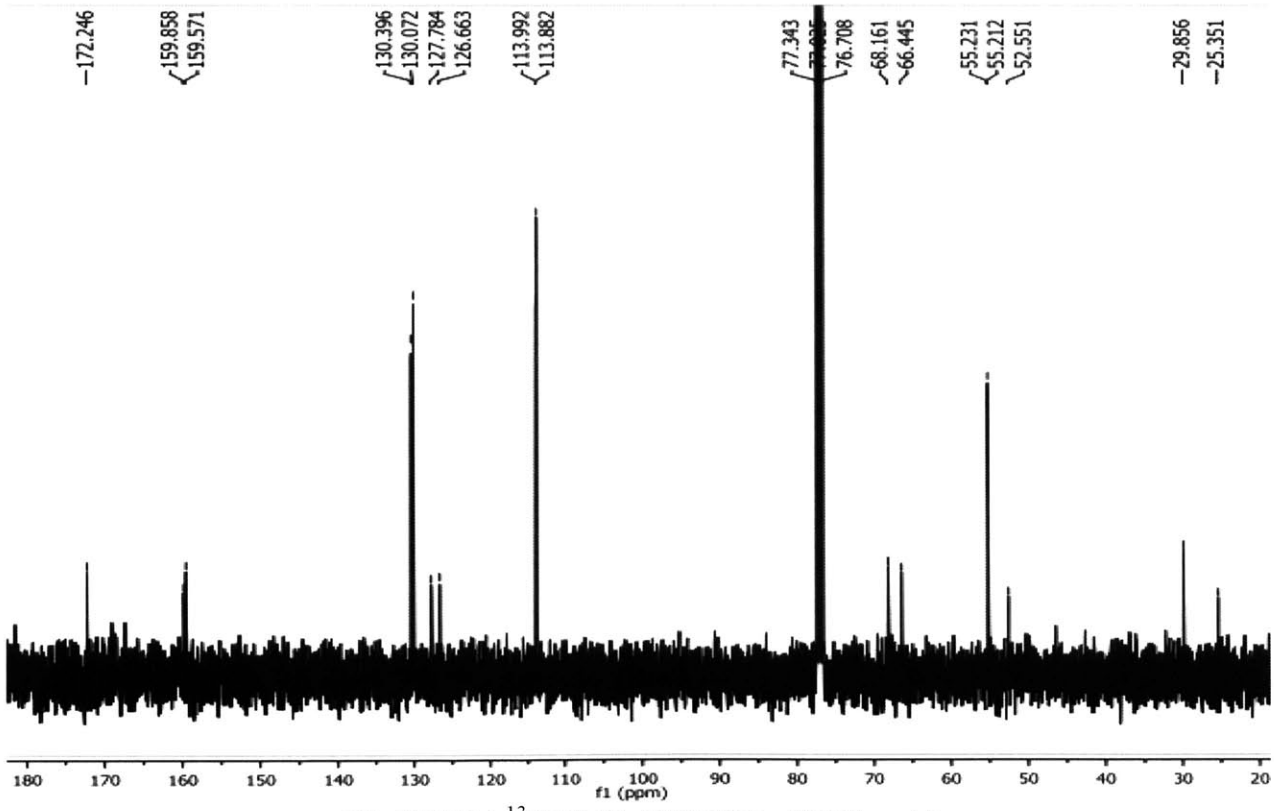

Glu(PMB$_2$) ^{13}C NMR (400 MHz, $CDCl_3$, r.t.)

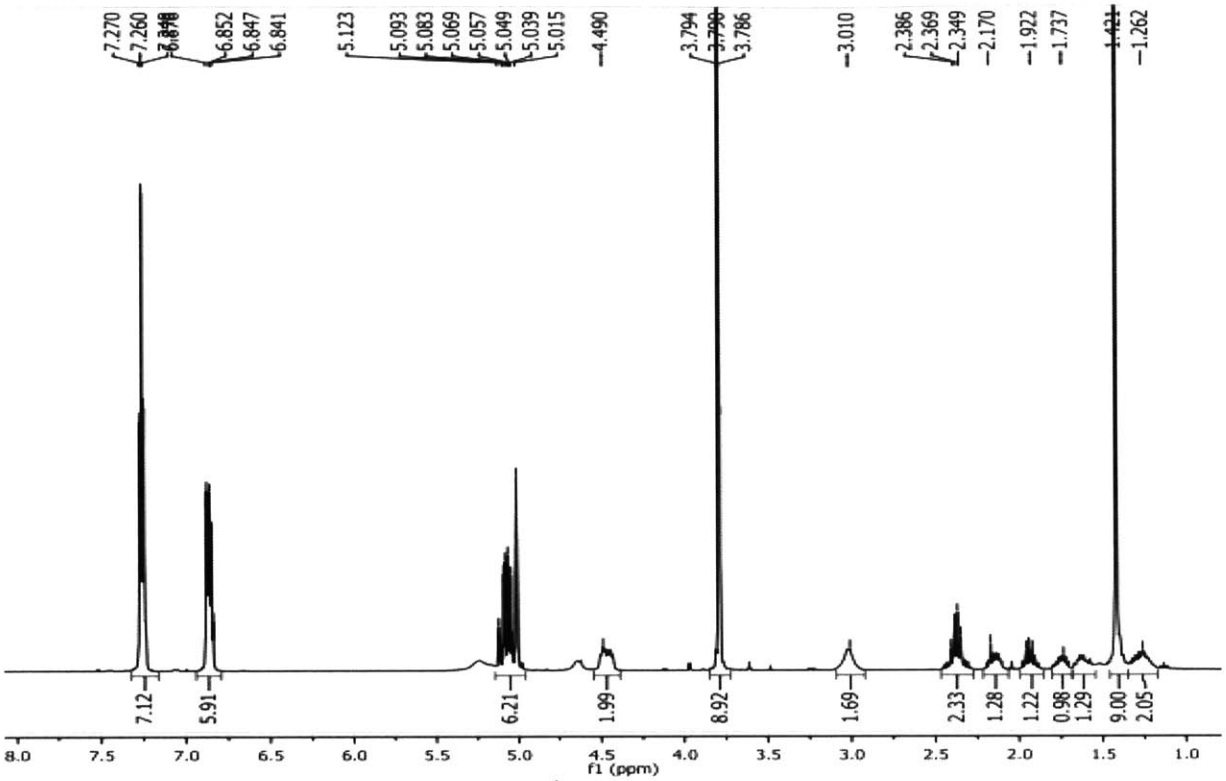

Boc-PMSA-PMB$_3$ ^{1}H NMR (400 MHz, $CDCl_3$, r.t.)

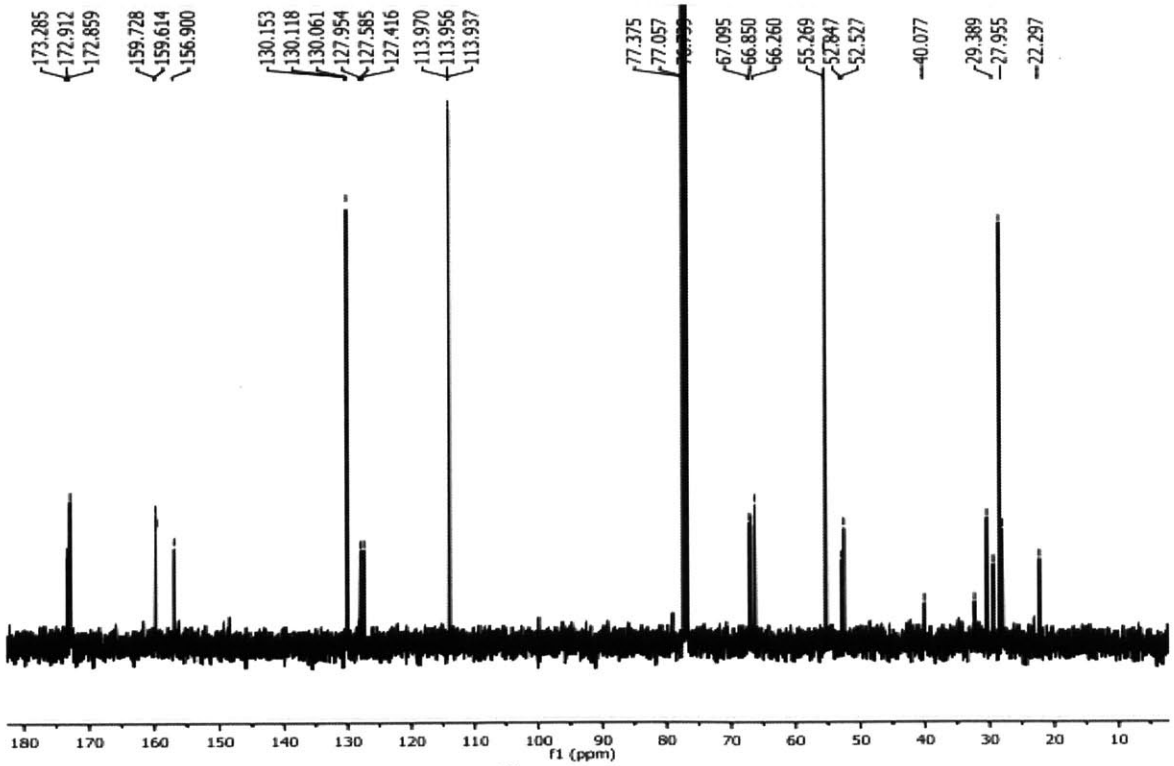

Boc-PMSA-PMB$_3$ ^{13}C NMR (400 MHz, $CDCl_3$, r.t.)

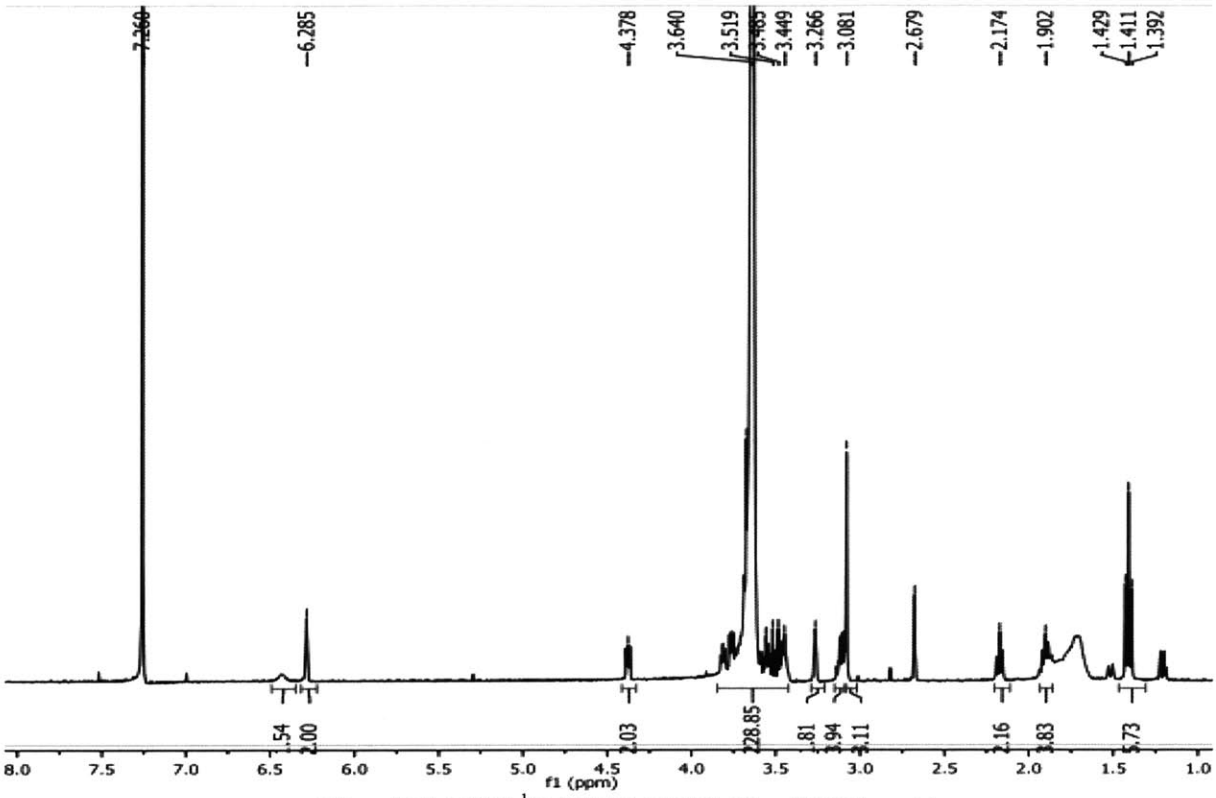

Mesyl 3k MM ^{1}H NMR (400 MHz, $CDCl_3$, r.t.)

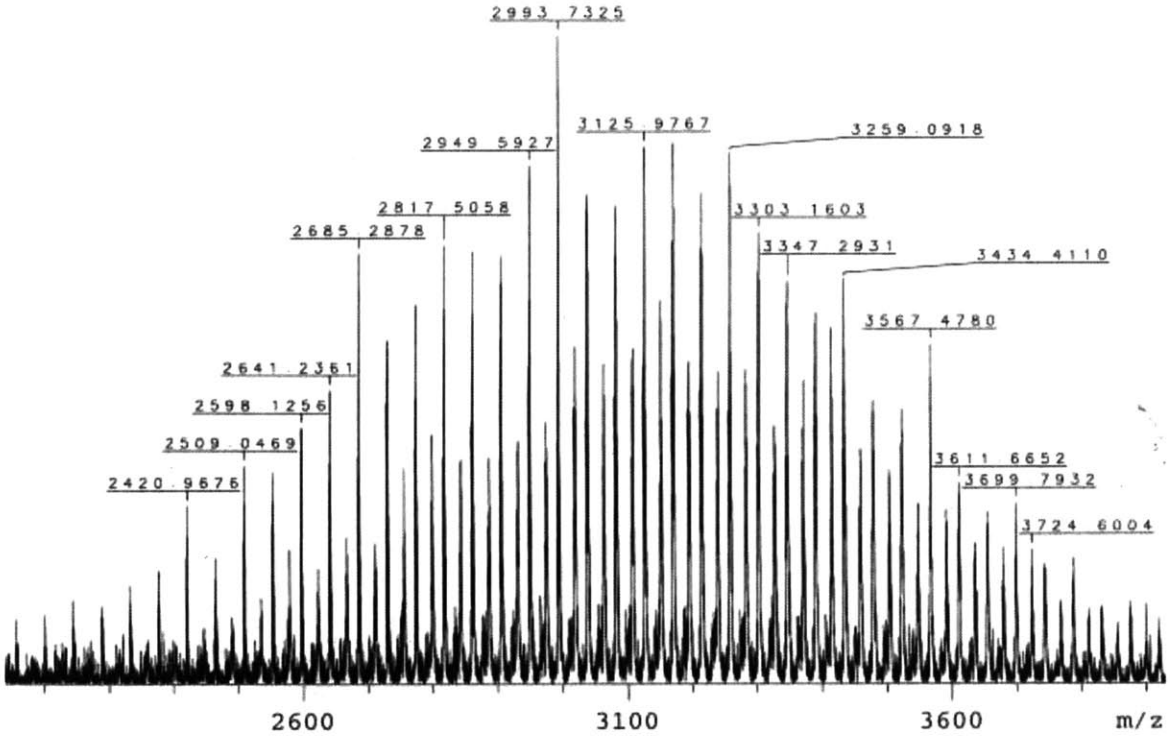

Mesyl 3k MM MALDI-TOF

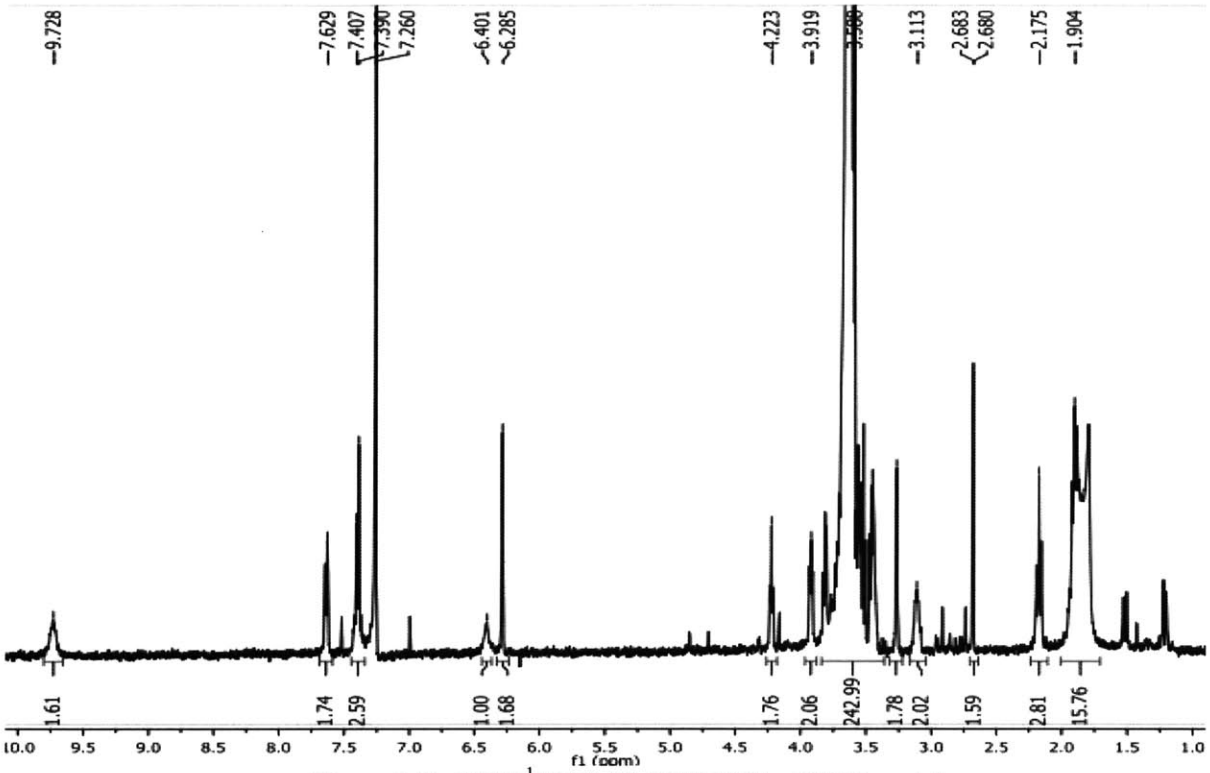

Benzyl 3k MM ^{1}H NMR (400 MHz, $CDCl_3$, r.t.)

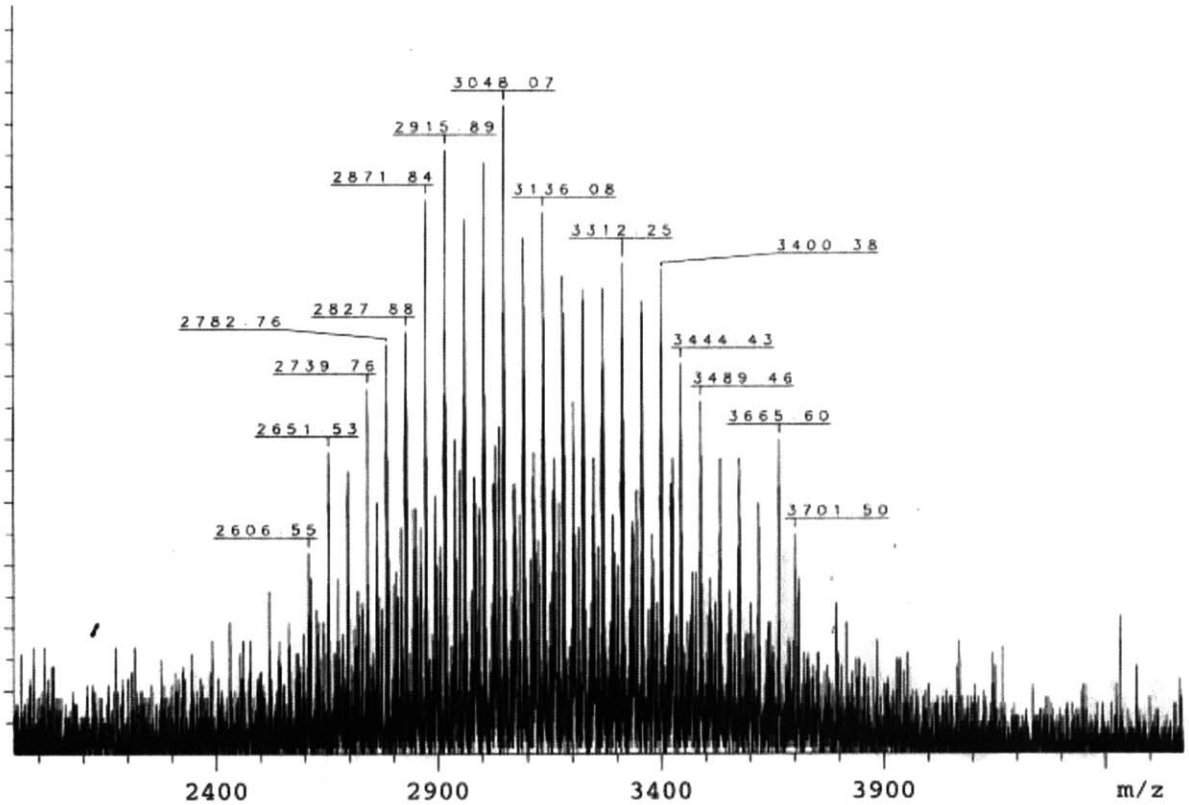

Benzyl 3k MM MALDI-TOF

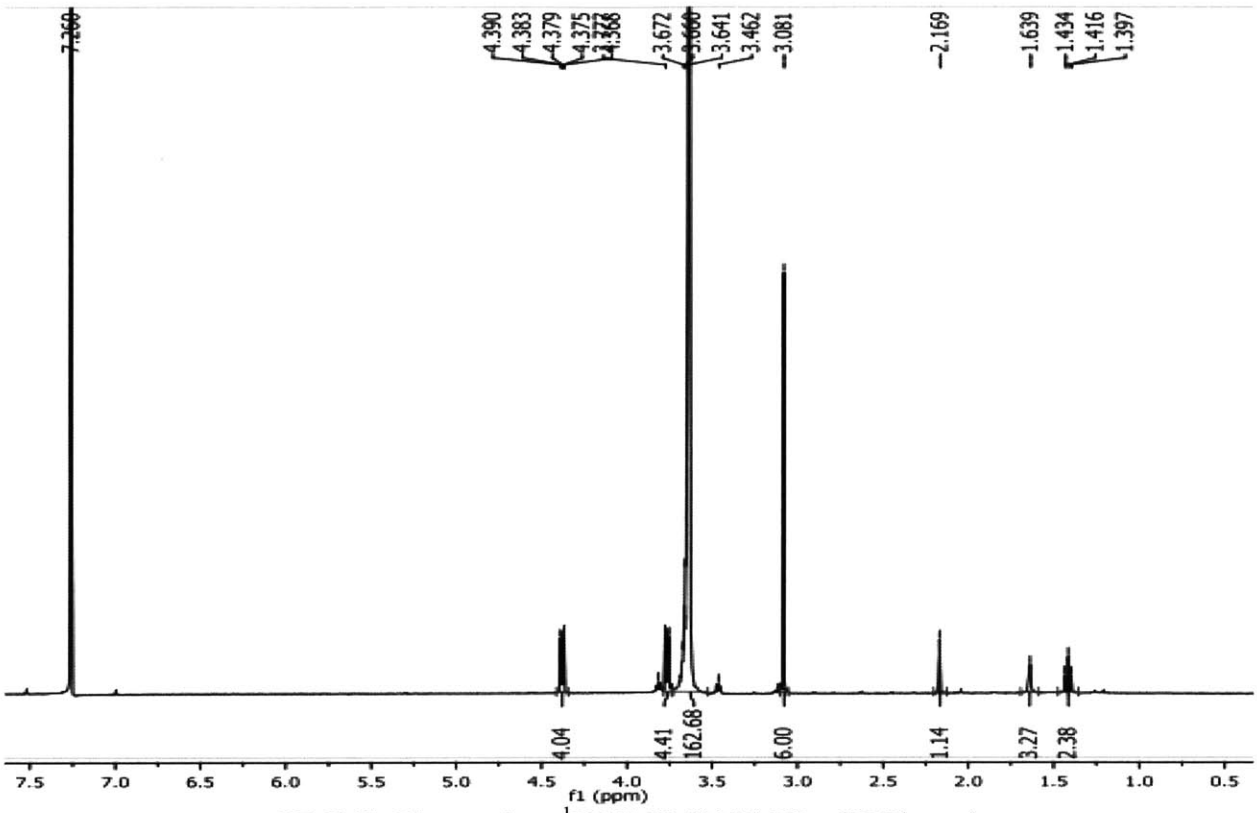

PEG 2k Bismesylate ^{1}H NMR (400 MHz, $CDCl_3$, r.t.)

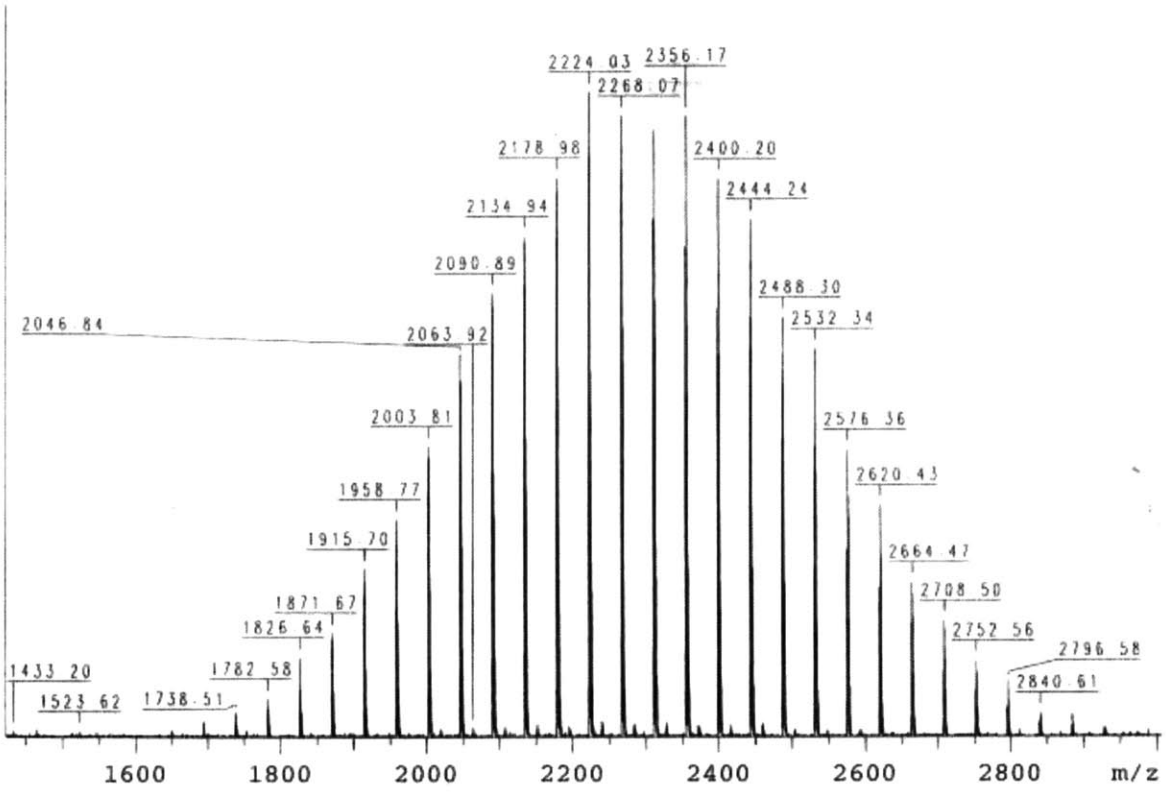

PEG 2k bismesylate MALDI-TOF

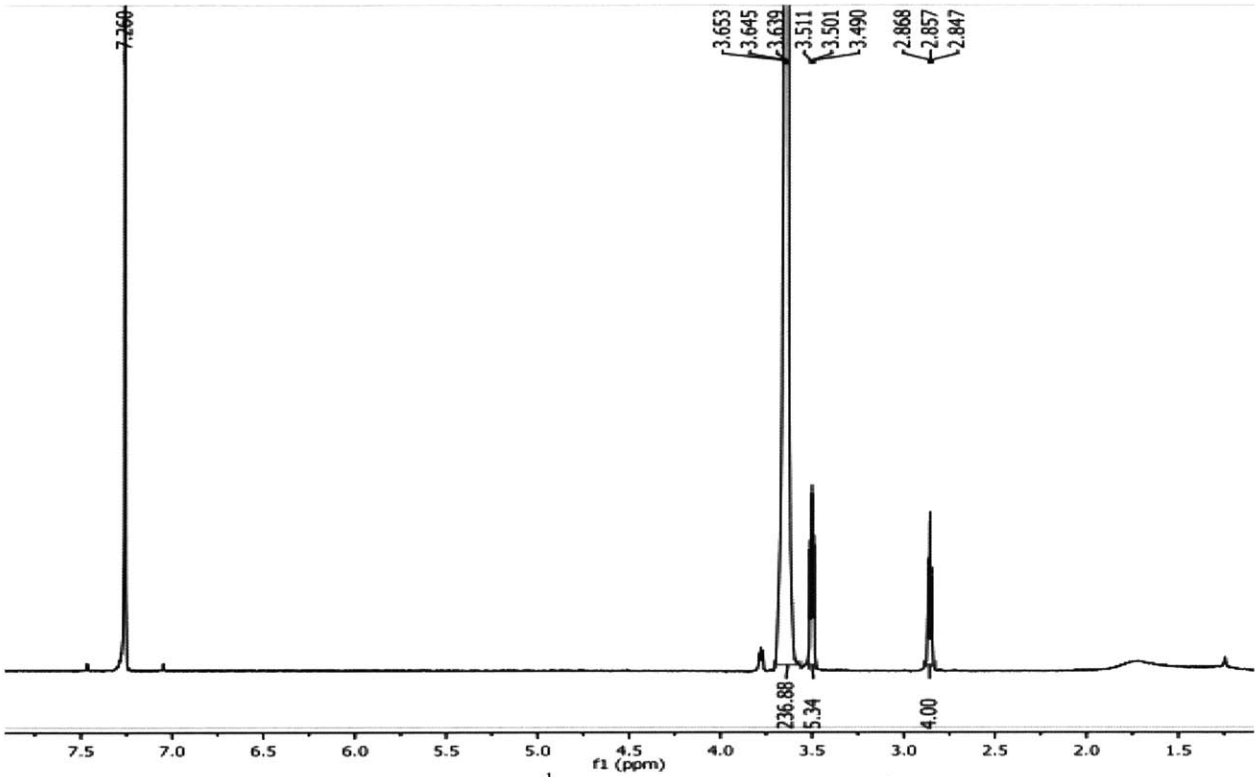

PEG 2k Bisamine ^{1}H NMR (400 MHz, $CDCl_3$, r.t.)

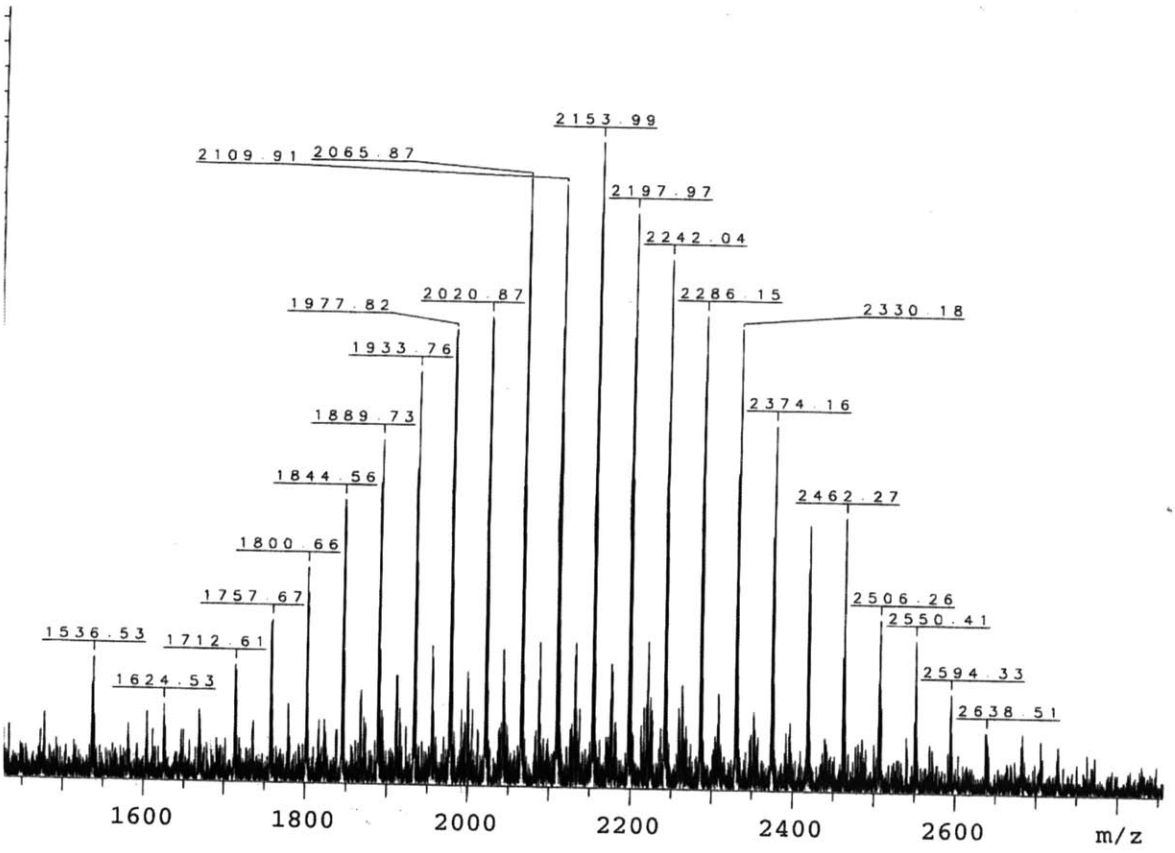

PEG 2k bisamine MALDI-TOF

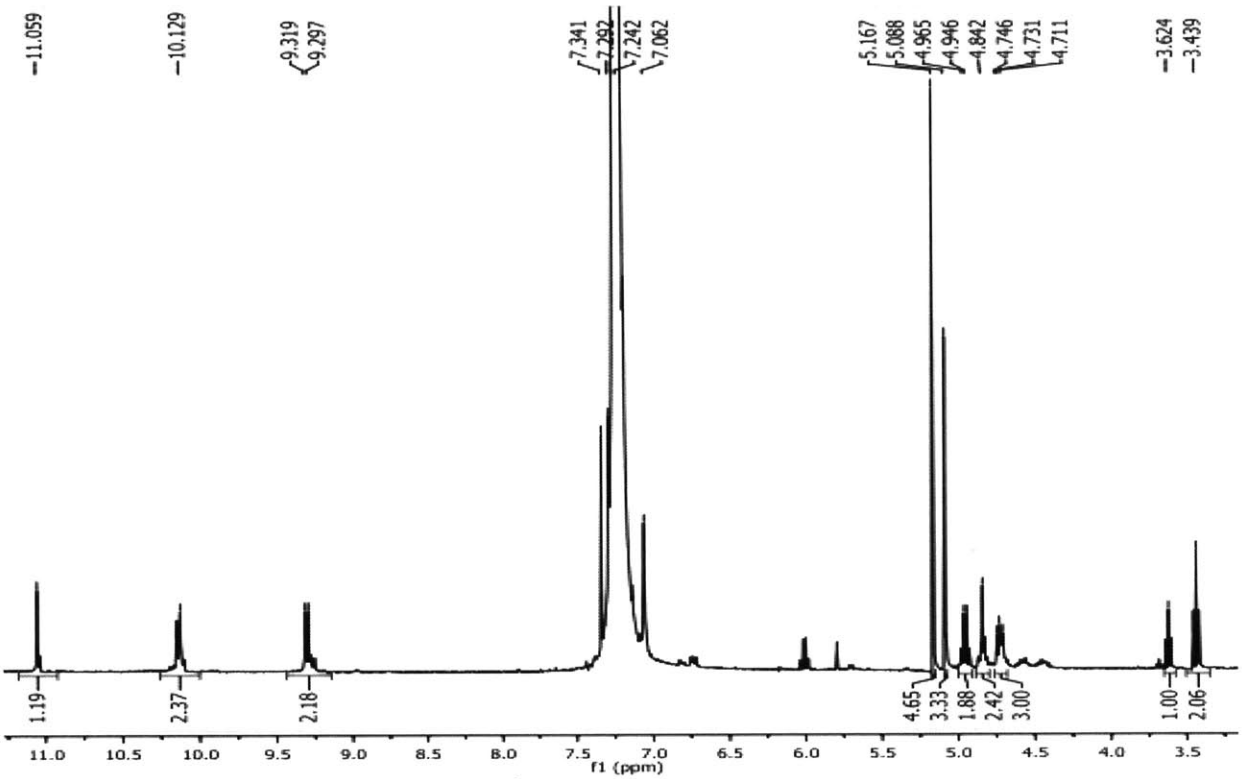

Folic acid NHS. ^{1}H NMR (400 MHz, DMSO-D_6, r.t.)

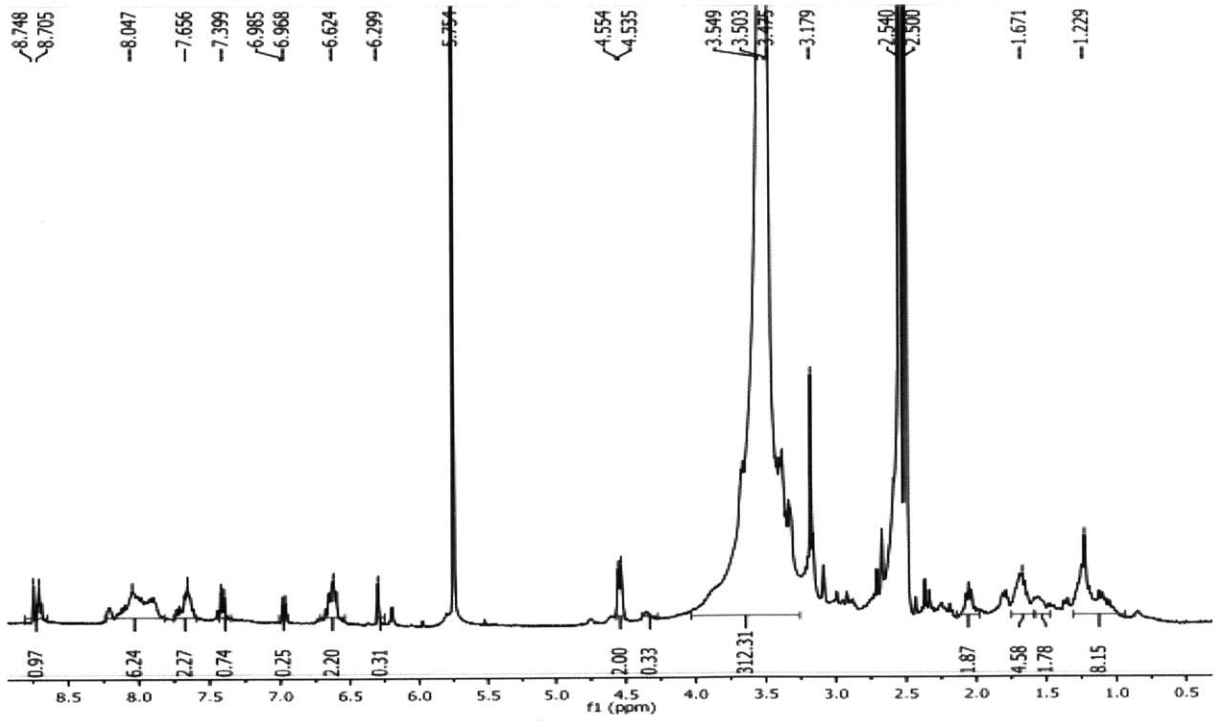

Folic acid 2k MM. ^{1}H NMR (400 MHz, DMSO-D_6, r.t.)

Chapter VI. References

1 Park, K. *et al.* New Generation of Multifunctional Nanoparticles for Cancer Imaging and Therapy. *Adv Funct Mater* **19**, 1553-1566, doi:Doi 10.1002/Adfm.200801655 (2009).

2 Doane, T. L. & Burda, C. The unique role of nanoparticles in nanomedicine: imaging, drug delivery and therapy. *Chem Soc Rev* **41**, 2885-2911, doi:Doi 10.1039/C2cs15260f (2012).

3 Thurecht, K. J. Polymers as Probes for Multimodal Imaging with MRI. *Macromol Chem Phys* **213**, 2567-2572, doi:Doi 10.1002/Macp.201200420 (2012).

4 Villaraza, A. J. L., Bumb, A. & Brechbiel, M. W. Macromolecules, Dendrimers, and Nanomaterials in Magnetic Resonance Imaging: The Interplay between Size, Function, and Pharmacokinetics. *Chem Rev* **110**, 2921-2959, doi:Doi 10.1021/Cr900232t (2010).

5 van Dam, G. M. *et al.* Intraoperative tumor-specific fluorescence imaging in ovarian cancer by folate receptor-alpha targeting: first in-human results. *Nat Med* **17**, 1315-U1202, doi:Doi 10.1038/Nm.2472 (2011).

6 Ghoroghchian, P. P. *et al.* Near-infrared-emissive polymersomes: Self-assembled soft matter for in vivo optical imaging. *P Natl Acad Sci USA* **102**, 2922-2927, doi:Doi 10.1073/Pnas.0409394102 (2005).

7 Deng, Z. J. *et al.* Layer-by-Layer Nanoparticles for Systemic Codelivery of an Anticancer Drug and siRNA for Potential Triple-Negative Breast Cancer Treatment. *Acs Nano* **7**, 9571-9584, doi:Doi 10.1021/Nn4047925 (2013).

8 Medarova, Z., Pham, W., Farrar, C., Petkova, V. & Moore, A. In vivo imaging of siRNA delivery and silencing in tumors. *Nat Med* **13**, 372-377, doi:Doi 10.1038/Nm1486 (2007).

9 Koyama, Y. *et al.* A dendrimer-based nanosized contrast agent, dual-labeled for magnetic resonance and optical fluorescence imaging to localize the sentinel lymph node in mice. *J Magn Reson Imaging* **25**, 866-871, doi:Doi 10.1002/Jmri.20852 (2007).

10 Olson, E. S. *et al.* Activatable cell penetrating peptides linked to nanoparticles as dual probes for in vivo fluorescence and MR imaging of proteases. *P Natl Acad Sci USA* **107**, 4311-4316, doi:Doi 10.1073/Pnas.0910283107 (2010).

11 Jiang, L. Y. *et al.* pH/temperature sensitive magnetic nanogels conjugated with Cy5.5-labled lactoferrin for MR and fluorescence imaging of glioma in rats. *Biomaterials* **34**, 7418-7428, doi:Doi 10.1016/J.Biomaterials.2013.05.078 (2013).

12 Rolfe, B. E. *et al.* Multimodal Polymer Nanoparticles with Combined 19F Magnetic Resonance and Optical Detection for Tunable, Targeted, Multimodal Imaging in Vivo. *J. Am. Chem. Soc.* **136**, 2413-2419, doi:10.1021/ja410351h (2014).

13 Wang, K. W., Peng, H., Thurecht, K. J., Puttick, S. & Whittaker, A. K. Biodegradable core crosslinked star polymer nanoparticles as F-19 MRI contrast agents for selective imaging. *Polym Chem-Uk* **5**, 1760-1771, doi:Doi 10.1039/C3py01311a (2014).

14 Tu, C., Nagao, R. & Louie, A. Y. Multimodal Magnetic-Resonance/Optical-Imaging Contrast Agent Sensitive to NADH. *Angew Chem Int Edit* **48**, 6547-6551, doi:Doi 10.1002/Anie.200900984 (2009).

15 Zhang, X. A., Lovejoy, K. S., Jasanoff, A. & Lippard, S. J. Water-soluble porphyrins imaging platform for MM zinc sensing. *P Natl Acad Sci USA* **104**, 10780-10785, doi:Doi 10.1073/Pnas.0702393104 (2007).

16 You, Y. M. *et al.* Manganese displacement from Zinpyr-1 allows zinc detection by fluorescence microscopy and magnetic resonance imaging. *Chem Commun* **46**, 4139-4141, doi:Doi 10.1039/C0cc00179a (2010).

17 Napolitano, R. *et al.* Synthesis and Relaxometric Characterization of a MRI Gd-Based Probe Responsive to Glutamic Acid Decarboxylase Enzymatic Activity. *J Med Chem* **56**, 2466-2477, doi:Doi 10.1021/Jm301831f (2013).

18 Davies, G. L., Kramberger, I. & Davis, J. J. Environmentally responsive MRI contrast agents. *Chem Commun* **49**, 9704-9721, doi:Doi 10.1039/C3cc44268c (2013).

19 Lauffer, R. B. Paramagnetic Metal-Complexes as Water Proton Relaxation Agents for Nmr Imaging - Theory and Design. *Chem Rev* **87**, 901-927, doi:Doi 10.1021/Cr00081a003 (1987).

20 Terreno, E., Delli Castelli, D., Viale, A. & Aime, S. Challenges for Molecular Magnetic Resonance Imaging. *Chem Rev* **110**, 3019-3042, doi:Doi 10.1021/Cr100025t (2010).

21 Butterworth, R. F., Spahr, L., Fontaine, S. & Layrargues, G. P. Manganese toxicity, dopaminergic dysfunction and hepatic encephalopathy. *Metab Brain Dis* **10**, 259-267, doi:Doi 10.1007/Bf02109357 (1995).

22 Braverman, I. & Cowper, S. Nephrogenic systemic fibrosis. *F1000 Med. Rep.* **2**, No. 84 (2010).

23 Swaminathan, S. *et al.* Nephrogenic systemic fibrosis, gadolinium, and iron mobilization. *New Engl J Med* **357**, 720-722, doi:Doi 10.1056/Nejmc070248 (2007).

24 Zhelev, Z. *et al.* Nitroxyl Radicals for Labeling of Conventional Therapeutics and Noninvasive Magnetic Resonance Imaging of Their Permeability for Blood-Brain Barrier: Relationship between Structure, Blood Clearance, and MRI Signal Dynamic in the Brain. *Mol Pharmaceut* **6**, 504-512, doi:Doi 10.1021/Mp800175k (2009).

25 Brasch, R. C. *et al.* Brain Nuclear Magnetic-Resonance Imaging Enhanced by a Paramagnetic Nitroxide Contrast Agent - Preliminary-Report. *Am J Roentgenol* **141**, 1019-1023 (1983).

26 Nagasaki, Y. Nitroxide radicals and nanoparticles: a partnership for nanomedicine radical delivery. *Therapeutic delivery* **3**, 165-179 (2012).

27 Rajca, A. *et al.* Organic Radical Contrast Agents for Magnetic Resonance Imaging. *Journal of the American Chemical Society* **134**, 15724-15727, doi:Doi 10.1021/Ja3079829 (2012).

28 Paletta, J. T., Pink, M., Foley, B., Rajca, S. & Rajca, A. Synthesis and Reduction Kinetics of Sterically Shielded Pyrrolidine Nitroxides. *Org Lett* **14**, 5322-5325, doi:Doi 10.1021/Ol3025061 (2012).

29 Burts, A. O. *et al.* Using EPR To Compare PEG-branch-nitroxide "Bivalent-Brush Polymers" and Traditional PEG Bottle–Brush Polymers: Branching Makes a Difference. *Macromolecules* **45**, 8310-8318, doi:10.1021/ma301874d (2012).

30 Johnson, J. A. *et al.* Drug-Loaded, Bivalent-Bottle-Brush Polymers by Graft-through ROMP. *Macromolecules (Washington, DC, United States)* **43**, 10326-10335 (2010).

31 Liu, J. *et al.* "Brush-First" Method for the Parallel Synthesis of Photocleavable, Nitroxide-Labeled Poly(ethylene glycol) Star Polymers. *Journal of the American Chemical Society* **134**, 16337-16344, doi:10.1021/ja3067176 (2012).

32 Johnson, J. A. *et al.* Core-Clickable PEG-Branch-Azide Bivalent-Bottle-Brush Polymers by ROMP: Grafting-Through and Clicking-To. *Journal of the American Chemical Society* **133**, 559-566 (2011).

33 Yapici, N. B. *et al.* New Rhodamine Nitroxide Based Fluorescent Probes for Intracellular Hydroxyl Radical Identification in Living Cells. *Org Lett* **14**, 50-53, doi:Doi 10.1021/Ol202816m (2012).

34 Ahn, H. Y. *et al.* Two-Photon Fluorescence Microscopy Imaging of Cellular Oxidative Stress Using Profluorescent Nitroxides. *Journal of the American Chemical Society* **134**, 4721-4730, doi:Doi 10.1021/Ja210315x (2012).

35 Medvedeva, N., Martin, V. V., Weis, A. L. & Likhtenshten, G. I. Dual fluorophore-nitronyl probe for investigation of superoxide dynamics and antioxidant status of biological systems. *J Photoch Photobio A* **163**, 45-51, doi:Doi 10.1016/S1010-6030(03)00430-1 (2004).

36 Micallef, A. S. *et al.* The application of a novel profluorescent nitroxide to monitor thermo-oxidative degradation of polypropylene. *Polym Degrad Stabil* **89**, 427-435, doi:Doi 10.1016/J.Polymdegradstab.2005.01.030 (2005).

37 Coenjarts, C. *et al.* Mapping photogenerated radicals in thin polymer films: Fluorescence imaging using a prefluorescent radical probe. *Journal of the American Chemical Society* **125**, 620-621, doi:Doi 10.1021/Ja028835s (2003).

38 Hilderbrand, S. A. & Weissleder, R. Near-infrared fluorescence: application to in vivo molecular imaging. *Current opinion in chemical biology* **14**, 71-79 (2010).

39 Vora, A., Singh, K. & Webster, D. C. A new approach to 3-miktoarm star polymers using a combination of reversible addition–fragmentation chain transfer (RAFT) and ring opening polymerization (ROP) via "Click" chemistry. *Polymer* **50**, 2768-2774 (2009).

40 Liao, L. *et al.* A Convergent Synthetic Platform for Single-Nanoparticle Combination Cancer Therapy: Ratiometric Loading and Controlled Release of Cisplatin, Doxorubicin, and Camptothecin. *Journal of the American Chemical Society* (2014).

41 Sato, S. *et al.* Synthesis and spectral properties of polymethine-cyanine dye–nitroxide radical hybrid compounds for use as fluorescence probes to monitor reducing species and radicals. *Spectrochimica Acta Part A: Molecular and Biomolecular Spectroscopy* **71**, 2030-2039, doi:http://dx.doi.org/10.1016/j.saa.2008.07.045 (2009).

42 Matko, J., Ohki, K. & Edidin, M. Luminescence Quenching by Nitroxide Spin Labels in Aqueous-Solution - Studies on the Mechanism of Quenching. *Biochemistry* **31**, 703-711, doi:Doi 10.1021/Bi00118a010 (1992).

43 Bobko, A. A., Kirilyuk, I. A., Grigor'ev, I. A., Zweier, J. L. & Khramtsov, V. V. Reversible reduction of nitroxides to hydroxylamines: Roles for ascorbate and glutathione. *Free Radical Bio Med* **42**, 404-412, doi:Doi 10.1016/J.Freeradbiomed.2006.11.007 (2007).

44 Workman, P. *et al.* Guidelines for the welfare and use of animals in cancer research. *British journal of cancer* **102**, 1555-1577 (2010).

45 Torchilin, V. Tumor delivery of macromolecular drugs based on the EPR effect. *Adv Drug Deliver Rev* **63**, 131-135, doi:Doi 10.1016/J.Addr.2010.03.011 (2011).

46 Vissers, M. C., Bozonet, S. M., Pearson, J. F. & Braithwaite, L. J. Dietary ascorbate intake affects steady state tissue concentrations in vitamin C-deficient mice: tissue deficiency after suboptimal intake and superior bioavailability from a food source (kiwifruit). *Am J Clin Nutr* **93**, 292-301, doi:10.3945/ajcn.110.004853 (2011).

47 Couet, W. R. *et al.* Pharmacokinetics and Metabolic-Fate of 2 Nitroxides Potentially Useful as Contrast Agents for Magnetic-Resonance Imaging. *Pharmaceut Res*, 203-209 (1984).

48 Raymond, K. N. & Pierre, V. C. Next Generation, High Relaxivity Gadolinium MRI Agents. *Bioconjugate Chemistry* **16**, 3-8 (2005).

49 Love, J. A., Morgan, J. P., Trnka, T. M. & Grubbs, R. H. A practical and highly active ruthenium-based catalyst that effects the cross metathesis of acrylonitrile. *Angewandte Chemie, International Edition* **41**, 4035-4037 (2002).

50 Herborn, C. U. *et al.* Clinical safety and diagnostic value of the gadolinium chelate gadoterate meglumine (Gd-DOTA). *Invest Radiol* **42**, 58-62 (2007).

51 Shellock, F. G. & Spinazzi, A. MRI Safety Update 2008: Part I, MRI Contrast Agents and Nephrogenic Systemic Fibrosis. *Am J Roentgenol* **191**, 1129-1139, doi:Doi 10.2214/Ajr.08.1038.1 (2008).

52 Caravan, P. Strategies for increasing the sensitivity of gadolinium based MRI contrast agents. *Chem Soc Rev* **35**, 512-523, doi:Doi 10.1039/B510982p (2006).

53 Caravan, P., Ellison, J. J., McMurry, T. J. & Lauffer, R. B. Gadolinium (III) chelates as MRI contrast agents: structure, dynamics, and applications. *Chem Rev* **99**, 2293-2352 (1999).

54 Wen, X. *et al.* Synthesis and characterization of poly (L-glutamic acid) gadolinium chelate: a new biodegradable MRI contrast agent. *Bioconjugate Chem* **15**, 1408-1415 (2004).
55 Erdogan, S., Roby, A., Sawant, R., Hurley, J. & Torchilin, V. P. Gadolinium-loaded polychelating polymer-containing cancer cell-specific immunoliposomes. *Journal of liposome research* **16**, 45-55 (2006).
56 Yan, Y., Such, G. K., Johnston, A. P. R., Lomas, H. & Caruso, F. Toward Therapeutic Delivery with Layer-by-Layer Engineered Particles. *Acs Nano* **5**, 4252-4257, doi:Doi 10.1021/Nn201793f (2011).
57 Swanson, S. D. *et al.* Targeted gadolinium-loaded dendrimer nanoparticles for tumor-specific magnetic resonance contrast enhancement. *Int J Nanomed* **3**, 201 (2008).
58 Kobayashi, H. *et al.* 3D-micro-MR angiography of mice using macromolecular MR contrast agents with polyamidoamine dendrimer core with reference to their pharmacokinetic properties. *Magnetic Resonance in Medicine* **45**, 454-460 (2001).
59 Luo, K. *et al.* Gadolinium-labeled peptide dendrimers with controlled structures as potential magnetic resonance imaging contrast agents. *Biomaterials* **32**, 7951-7960 (2011).
60 Kobayashi, H. *et al.* Macromolecular MRI contrast agents with small dendrimers: pharmacokinetic differences between sizes and cores. *Bioconjugate Chem* **14**, 388-394 (2003).
61 Rowe, M. D., Thamm, D. H., Kraft, S. L. & Boyes, S. G. Polymer-modified gadolinium metal-organic framework nanoparticles used as multifunctional nanomedicines for the targeted imaging and treatment of cancer. *Biomacromolecules* **10**, 983-993 (2009).
62 Grogna, M. *et al.* Polymer micelles decorated by gadolinium complexes as MRI blood contrast agents: design, synthesis and properties. *Polym Chem-Uk* **1**, 1485-1490 (2010).
63 Ananta, J. S. *et al.* Geometrical confinement of gadolinium-based contrast agents in nanoporous particles enhances T1 contrast. *Nature nanotechnology* **5**, 815-821 (2010).
64 Kim, J.-H. *et al.* Polymers for bioimaging. *Progress in Polymer Science* **32**, 1031-1053 (2007).
65 Tweedle, M. F., Hagan, J. J., Kumar, K., Mantha, S. & Chang, C. A. Reaction of Gadolinium Chelates with Endogenously Available Ions. *Magnetic Resonance Imaging* **9**, 409-415 (1991).
66 Farokhzad, O. C. *et al.* Targeted nanoparticle-aptamer bioconjugates for cancer chemotherapy in vivo. *Proceedings of the National Academy of Sciences* **103**, 6315-6320 (2006).
67 Hrkach, J. *et al.* Preclinical development and clinical translation of a PSMA-targeted docetaxel nanoparticle with a differentiated pharmacological profile. *Science translational medicine* **4**, 128ra139-128ra139 (2012).
68 Bagalkot, V., Farokhzad, O. C., Langer, R. & Jon, S. An Aptamer–Doxorubicin Physical Conjugate as a Novel Targeted Drug-Delivery Platform. *Angewandte Chemie International Edition* **45**, 8149-8152 (2006).
69 Nasongkla, N. *et al.* cRGD-functionalized polymer micelles for targeted doxorubicin delivery. *Angewandte Chemie* **116**, 6483-6487 (2004).
70 Huang, X. *et al.* A reexamination of active and passive tumor targeting by using rod-shaped gold nanocrystals and covalently conjugated peptide ligands. *Acs Nano* **4**, 5887-5896 (2010).
71 Brannon-Peppas, L. & Blanchette, J. O. Nanoparticle and targeted systems for cancer therapy. *Adv Drug Deliver Rev* **64**, 206-212 (2012).
72 Lu, Y. & Low, P. S. Folate-mediated delivery of macromolecular anticancer therapeutic agents. *Adv Drug Deliver Rev* **64**, 342-352 (2012).
73 Maeda, H., Wu, J., Sawa, T., Matsumura, Y. & Hori, K. Tumor vascular permeability and the EPR effect in macromolecular therapeutics: a review. *J Control Release* **65**, 271-284 (2000).
74 Danhier, F., Feron, O. & Préat, V. To exploit the tumor microenvironment: Passive and active tumor targeting of nanocarriers for anti-cancer drug delivery. *J Control Release* **148**, 135-146 (2010).

75 Peer, D. *et al.* Nanocarriers as an emerging platform for cancer therapy. *Nature nanotechnology* **2**, 751-760 (2007).

76 Dai, X., Su, Z. & Liu, J. O. An improved synthesis of a selective αβ3-integrin antagonist cyclo(RGDfK). *Tetrahedron Letters* **41**, 6295-6298 (2000).

77 Banerjee, S. R. *et al.* Synthesis and Evaluation of Technitium-99m- and Rhenium-Labeled Inhibitors of the Prostate-Specific Membrane Antigen (PSMA). *J. Med. Chem.* **51**, 4504-4517 (2008).

78 Choi, H. S. *et al.* Design considerations for tumour-targeted nanoparticles. *Nature nanotechnology* **5**, 42-47 (2009).

79 Pichavant, L., Bourget, C., Durrieu, M.-C. & Héroguez, V. Synthesis of pH-sensitive particles for local delivery of an antibiotic via dispersion ROMP. *Macromolecules* **44**, 7879-7887 (2011).

80 Tezgel, A. O., Telfer, J. C. & Tew, G. N. De novo designed protein transduction domain mimics from simple synthetic polymers. *Biomacromolecules* **12**, 3078-3083, doi:10.1021/bm200694u (2011).

81 Pack, D. W., Hoffman, A. S., Pun, S. & Stayton, P. S. Design and development of polymers for gene delivery. *Nature reviews. Drug discovery* **4**, 581-593, doi:10.1038/nrd1775 (2005).

82 Mitchell, D., Steinman, L., Kim, D., Fathman, C. & Rothbard, J. Polyarginine enters cells more efficiently than other polycationic homopolymers. *The Journal of Peptide Research* **56**, 318-325 (2000).

83 Melikov, K. & Chernomordik, L. Arginine-rich cell penetrating peptides: from endosomal uptake to nuclear delivery. *Cellular and Molecular Life Sciences CMLS* **62**, 2739-2749 (2005).

84 Kim, S. H., Jeong, J. H., Chun, K. W. & Park, T. G. Target-specific cellular uptake of PLGA nanoparticles coated with poly (L-lysine)-poly (ethylene glycol)-folate conjugate. *Langmuir* **21**, 8852-8857 (2005).

85 Wender, P. A. *et al.* The design, synthesis, and evaluation of molecules that enable or enhance cellular uptake: peptoid molecular transporters. *Proceedings of the National Academy of Sciences* **97**, 13003-13008 (2000).

86 Poon, Z., Chang, D., Zhao, X. & Hammond, P. T. Layer-by-layer nanoparticles with a pH-sheddable layer for in vivo targeting of tumor hypoxia. *Acs Nano* **5**, 4284-4292 (2011).

87 Morton, S. W., Poon, Z. & Hammond, P. T. The architecture and biological performance of drug-loaded LbL nanoparticles. *Biomaterials* **34**, 5328-5335, doi:10.1016/j.biomaterials.2013.03.059 (2013).

88 Luo, Y., Bernshaw, N. J., Lu, Z.-R., Kopecek, J. & Prestwich, G. D. Targeted delivery of doxorubicin by HPMA copolymer-hyaluronan bioconjugates. *Pharmaceut Res* **19**, 396-402 (2002).

89 Lee, R. J. & Low, P. S. Folate-mediated tumor cell targeting of liposome-entrapped doxorubicin in vitro. *Biochimica et Biophysica Acta (BBA)-Biomembranes* **1233**, 134-144 (1995).

90 Guo, W. & Lee, R. J. Receptor-targeted gene delivery viafolate-conjugated polyethylenimine. *Aaps Pharmsci* **1**, 20-26 (1999).